nature portfolio

Peer Review File

Ion-Triggered Reconfigurable Hydrogel with Salt-Enhanced Mechanical and Swelling Properties via Network Topological Adaptation

Corresponding Author: Professor Liyuan Zhang

This file contains all reviewer reports in order by version, followed by all author rebuttals in order by version.

Version 0:

Reviewer comments:

Reviewer #1

(Remarks to the Author)
The manuscript reported a double network hydrogel composed of poly(AMPS) and zwitterionic AM-SBVI that strengthens while swelling in brine. Upon salt exposure, the network undergoes ion-triggered topological reconfiguration, the intrachain zwitterionic loops open and re-form as inter-network SBVI+-AMPS- bridges, which yields a higher effective bridge density ve, at lower polymer fraction (Φ). The hydrogel demonstrates a 3.4-fold increase in tensile strength and a 2.1-fold enhancement in equilibrium swelling ratio in 200 g/L NaCl compared to deionized water. SAXS and XPS confirm the ion-mediated decoupling of crosslinking domains and redistribution of charge density. Moreover, simulation calculations suggest more strong interactions between SBVI and AMPS under high salinity water. Coreflooding experiment demonstrates robust injectability and flow-resistance characteristics under high salinity porous rock. I suggest the publication of this manuscript with major revision upon addressing the following comments.
1. There are some descriptions related to tensile strength and equilibrium swelling ratio in the main manuscript that the reviewer cannot find the related supporting data.
2. In the abstract section, Fig. S8, the hydrogel demonstrates a 3.4-fold increase in tensile strength and a 2.1-fold enhancement in equilibrium swelling ratio in 200 g/L NaCl compared to deionized water. The authors need to specify the data that supported the 3.4-fold increase in tensile strength and 2.1-fold enhancement in equilibrium swelling ratio.
3. There are many hydrogel samples being tested as shown in the figures. The authors need to specify the feed molar ratio of monomers, feed molar ratio of first and second networks, concentration of crosslinking agents and other parameters for preparing the hydrogel samples in the figure legends.
4. Line 212-215, the authors claimed that DAMPS/AM-SBVI hydrogels immersed in 200 g/L NaCl exhibit tensile stress of 0.33 MPa and strain of 123%, which are significantly higher than those of water-swollen hydrogels (Figure 2C-E). However, based on Figure 2D, the strain of DAMPS/AM-SBVI hydrogels immersed in 200 g/L NaCl was only about 79%.
5. Based on Table S2, the molar ratio of AM in the second network is high. That said, the noncovalent interactions exerted by AM should play some role on the morphology and physical properties of the network. The formation of hydrogen bonding, cation-dipole, and other interactions between the AM and other monomers upon salt exposure would also trigger the changes in the network morphology, swelling, and mechanical properties. This effect should be discussed and the related experiments and simulations should be conducted to elucidate the mechanism.
6. The enhancement of both hydrogel mechanical strength and swelling performance is very complex. The authors mainly attributed it to a stronger interaction between SBVI and AMPS under high salinity water simply based on the simulation calculation. There might be several mechanisms that contributed to the enhancement. For example, it is possible that, upon salt exposure, the hydrogen bonding, cation-dipole, and other interactions between the AM and other monomers were screened and triggered the rearrangement of polymeric network and increase of ionic/nonionic bridging, partly contributing to network stability and salt-enhanced elasticity.

Reviewer #2

(Remarks to the Author)
This manuscript reports a double-network hydrogel composed of poly(AMPS) and poly(SBVI-co-Am) networks, which

exhibits salt-enhanced mechanical properties. While the mechanical performance and structure of the gel are investigated, several critical issues must be addressed before the work can be considered for publication.
1.The introduction section is rather confusing. Whether for zwitterionic polymers or other types of polymers, most undergo changes in network structure and mechanical properties in saline environments. The authors have not adequately categorized or elaborated on these aspects. Moreover, when reading these paragraphs, it is difficult to discern the authors' intention: Is the goal to obtain gels with unchanged mechanical properties in brine, or to develop gels with enhanced performance in brine? If the latter, there have already been numerous reports of ion-enhanced cases in various polymer systems, including single-charged polymers, zwitterionic polymers, and non-ionic polymers. Therefore, the authors need to highlight the innovation and uniqueness of this work.
2.There are many zwitterionic monomers, the reason for choosing SBVI should be clarified properly. It is very important to illustrate the design method of materials.
3.In the text, the abbreviation appeared first time should have its full name. For example, the “EOR” at line 71, page 4.
4.The shape of the tensile stress-strain curve appears unusual, as a plateau is observed in the later stage of stretching. This differs from the typical behavior of glass materials, elastomers, and gels. Could this be due to the gel sample gradually slipping from the grips of the tensile machine? The authors need to provide an explanation for this phenomenon.
5.The Young’s modulus of the gels with varying conditions should be calculated and comparied, which was associated with cross-linking density of the network. Besides, it is also suggest to compare Young’s modulus with shear modulus.
6.In Figure 1G, the comparison with single-network samples that equilibrated in water is of limited significance, as the effectiveness of the double-network in enhancing the toughness of hydrogels has already been well-established through repeated demonstrations after 2003. Instead, to clarify the key mechanism of this work, the mechanical performance, structural changes, and swelling behavior of each single-network gel component in saline water should be examined and thoroughly compared.

Reviewer #3

(Remarks to the Author)
In this manuscript, the authors developed an innovative ion-triggered reconfigurable hydrogel through a double network system composed of AMPS/AM-ABVI, fabricating DAMPS/AM-ABVI hydrogels. These hydrogels demonstrated paradoxical salt-enhanced mechanical performance and swelling behavior. The researchers also provided an excellent mechanistic analysis of the salt-induced adaptive structural reorganization, revealing that inner-chain ion-pair loops dynamically unlock and reform as intra-network bridges (SBVI+-AMPS-) that serve as load-bearing elements under mechanical stress. Furthermore, the authors developed a temporary plugging agent based on DAMPS/AM-SBVI hydrogels and systematically investigated its coreflooding plugging efficiency and degradation performance, demonstrating its promising potential for applications in heterogeneous reservoirs, particularly under high-salinity and high-temperature conditions.
I think the work is very interesting and potentially worthy of publication in Nature Communications. However, the author still needs to revise the draft and answer some question prior to acceptance:

1. The text part needs to be double-checked. The phrase "A deep analysis concerts swelling/rheology into three descriptors, v_e, χ (Flory-Rehner inversion), and floop (loop fraction from bridge capacity)" needs clarification.

2. What were the theoretical or experimental bases for optimizing various parameters during the preparation of this DAMPS/AM-SBVI double-network hydrogel?

3. While SBVI is described as a laboratory-synthesized zwitterionic monomer, details regarding its synthesis procedure are notably absent in the manuscript.

4. Why was the Flory-Rehner equation selected over alternative models (e.g., the Beltman-modified model) for χ parameter calculation? Does electrostatic shielding under high-salinity conditions potentially interfere with this model's applicability?

5. What is the justification for setting ζ=1 in the equation ve=G'/ζRT?

6. The equation needs to be double-checked, F_ion=RT ∑ _i⁣〖 c_i^b (e^(-z_i u) (-z_i u-1)〗 +1).

7. 'SBVI++AMPS-' contains incorrect superscript/subscript formatting.

8. Regarding free energy decomposition, what is the rationale for neglecting the Fdiss term? Detailed data supporting Figure 3L should be supplemented.

Numerous studies have also reported various functional zwitterionic hydrogels. To better highlight this work's novelty, a comparative analysis emphasizing the material's distinctive advantages over existing zwitterionic hydrogels should be included.

10. Other minor: such as in Figure 2C, the pictures demonstrating the tensile stress-strain tests of swollen hydrogels are presented without a scale bar.
Some figure caption needs to be double checked.
In the supporting information, the character of SBVI needs to be provide, such as NMR.

Version 1:

Reviewer comments:

Reviewer #1

(Remarks to the Author)
The authors have addressed the reviewers' comments. I suggest teh publication of this manuscript in Nature Communcations.

Reviewer #2

(Remarks to the Author)
It can be accepted as this version.

Reviewer #3

(Remarks to the Author)
After careful review of the revised manuscript, all concerns raised in the previous review have been adequately addressed, and the paper is recommended for acceptance.

REVIEWER COMMENTS

Reviewer #1 (Remarks to the Author):

The manuscript reported a double network hydrogel composed of poly(AMPS) and zwitterionic AM-SBVI that strengthens while swelling in brine. Upon salt exposure, the network undergoes ion-triggered topological reconfiguration, the intrachain zwitterionic loops open and re-form as inter-network SBVI+-AMPS- bridges, which yields a higher effective bridge density ve, at lower polymer fraction (Φ). The hydrogel demonstrates a 3.4-fold increase in tensile strength and a 2.1-fold enhancement in equilibrium swelling ratio in 200 g/L NaCl compared to deionized water. SAXS and XPS confirm the ion-mediated decoupling of crosslinking domains and redistribution of charge density. Moreover, simulation calculations suggest more strong interactions between SBVI and AMPS under high salinity water. Coreflooding experiment demonstrates robust injectability and flow-resistance characteristics under high salinity porous rock. I suggest the publication of this manuscript with major revision upon addressing the following comments.

1. There are some descriptions related to tensile strength and equilibrium swelling ratio in the main manuscript that the reviewer cannot find the related supporting data.

Thank you for your careful review. We have now provided detailed data support and comprehensive explanations regarding the tensile strength and equilibrium swelling ratio.

About the equilibrium swelling ratio, we investigate the swelling behavior of the hydrogels in deionized water and various saline solutions. The swelling ratio (S_r) is employed for quantitative characterization, calculated using the following equation:

$$S_r = \frac{D_t^2 H_t - D_0^2 H_0}{D_0^2 H_0}$$

D_0 is the radius of the original cylindrical hydrogel sample; H_0 is the thickness of the original cylindrical hydrogel sample; D_t is the radius of the hydrogel after immersion for time t; H_t is the thickness of the hydrogel after immersion for time t.

S_r reflects the volumetric changes of the hydrogels, and the experimental results under different solvent environments are presented in Figure R1. The results demonstrate that during the initial 131 min, the hydrogel exhibits a faster swelling rate in water, with S_r values exceeding those in saline solutions. From 131 min to 303 min, the S_r in water gradually stabilizes and reaches swelling equilibrium, with a maximum value of approximately 17.63. During this period, the swelling rate of S_r in saline solutions gradually increases and eventually surpasses that in water. After 303 min of swelling, the S_r values in all saline solutions surpassed those in water. Following 367 min of swelling, the Sr in saline solutions gradually stabilizes and reaches swelling equilibrium. These results indicate that in water, the highly charged AMPS network promotes volumetric expansion through osmotic pressure-driven swelling, resulting in higher S_r values than in saline solutions during the initial 131 min. Specifically, as illustrated in Figure R2, the S_r of the single-network S_{AMPS} is 2.45 times that of $S_{AM\text{-}SBVI}$ in water, confirming the contribution of AMPS to swelling performance in aqueous environments.

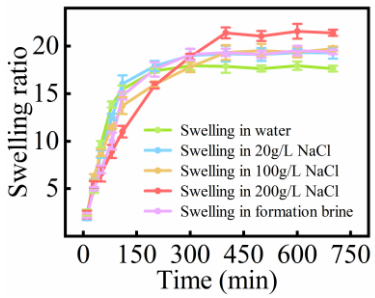

Figure R1. The S_r of hydrogels swelling in different solvent environments

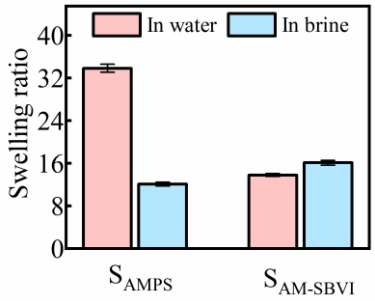

Figure R2. The swelling ratio comparison of S_{AMPS} and $S_{AM\text{-}SBVI}$

Generally, salt ions can shield the electrostatic interactions between polymer chains, typically resulting in reduced swelling performance in saline solutions, with higher salt concentrations leading to more pronounced swelling suppression.

Consequently, conventional hydrogels usually exhibit varying degrees of swelling reduction in saline environments compared to pure water. Remarkably, however, the S_r values of our hydrogels ($D_{AMPS/AM\text{-}SBVI}$) in water, 20 g/L NaCl, 100 g/L NaCl, 200g/L NaCl, and formation brine are 17.63, 19.28, 19.74, 21.41, and 19.38, respectively. $D_{AMPS/AM\text{-}SBVI}$ demonstrate superior swelling performance in saline solutions compared to pure water, achieving an anomalous salt-enhanced swelling property.

To further substantiate this anomalous salt-enhanced swelling behavior, the water content (W_r) of the hydrogels is evaluated under different solvent environment, calculated using the following equation:

$$W_r = \frac{M_t - M_0}{M_0}$$

M_0 represents the initial gel mass prior to swelling; M_t denotes the gel mass after swelling for time t.

W_r reflects the water retention capacity of the hydrogels, as shown in Figure R3. The trend of W_r is closely consistent with that of S_r. Initially, W_r in water exceeded that in saline solutions, while at later stages of swelling, W_r in saline solutions progressively surpassed that in pure water.

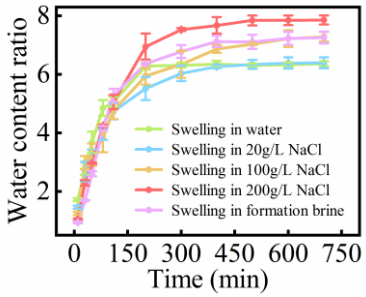

Figure R3. The W_r of hydrogels swelling in different solvent environments

Furthermore, our hydrogels $D_{AMPS/AM\text{-}SBVI}$ exhibit an abnormal swelling enhancement with increasing salt concentration. The S_r in 200 g/L NaCl exhibits an 11.05% increase compared to that in 20 g/L NaCl. The maximum W_r of 7.87 is observed in 200 g/L NaCl, representing a 24.4% increase compared to pure water. This anomalous salt-enhanced swelling suggests a conformational transition in the

AM-SBVI network, where the anti-polyelectrolyte effect dominates, promoting hydrogel expansion and increased water uptake in saline environments (Figure R4). This transition from a collapsed conformation in pure water to an extended conformation in saline solutions enables the salt-tolerant hydrogel $D_{AMPS/AM-SBVI}$ to avoid the typical collapse phenomenon exhibited by conventional polyelectrolyte hydrogels in saline environments[1, 2].

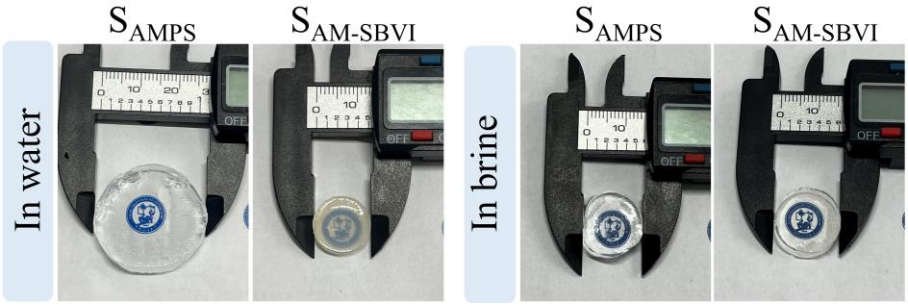

Figure R4. Photographs of hydrogels after swelling in different environments

Traditional hydrogels typically experience mechanical deterioration due to polymer chain dilution and network weakening upon swelling in brine[3, 4], with electrolyte presence exacerbating mechanical loss and even causing structural disintegration of swollen hydrogels. To evaluate the mechanical performance of the prepared hydrogels post-swelling, dumbbell-shaped specimens are prepared and allowed to reach swelling equilibrium in different solvents. Tensile tests are conducted using a universal testing machine at a constant crosshead speed of 20 mm/min, with stress-strain values recorded throughout the measurement. The stress-strain curves of hydrogels after swelling in various solvents are shown in Figure R5.

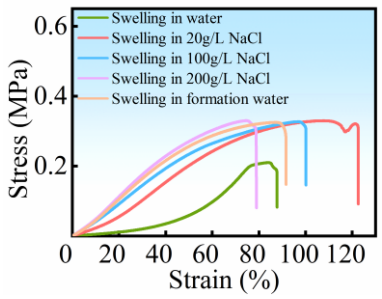

Figure R5. Stress-strain curves of hydrogels after swelling in different environments

After swelling, the hydrogels exhibit stress/strain values of 0.19 MPa/87.76% in water, 0.31 MPa/122.3% in 20 g/L NaCl, 0.31 MPa/100.2% in 100 g/L NaCl, 0.31 MPa/78.9% in 200 g/L NaCl, and 0.31 MPa/91.4% in formation brine. Notably, the

$D_{AMPS/AM-SBVI}$ hydrogels show 63.16% higher stress values across all saline solutions compared to pure water, with the strain values in saline solutions showed a maximum increase of 39.36% compared to water.

The toughness is calculated by integrating the area under the stress-strain curve, as shown in Figure R6. The toughness values after swelling in water, 20 g/L NaCl, 100 g/L NaCl, 200 g/L NaCl, and formation brine are 5.98, 26.02, 20.34, 15.19, and 18.59 MJ/m^3, respectively. Notably, the toughness of hydrogels swollen in 20g/L NaCl exhibits a 335.12% increase compared to those in pure water, surpassing previously reported systems with comparable swelling characteristics[5, 6]. These results demonstrate the salt-induced mechanical enhancement of salt-tolerant hydrogels after swelling in varying salt concentration environments.

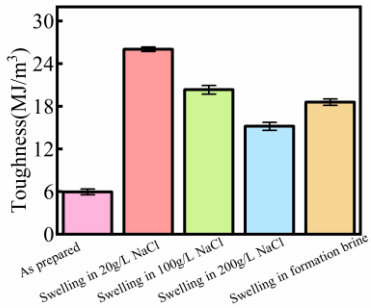

Figure R6. The toughness of hydrogels after swelling in different environments

When immersed in formation brine containing Ca^{2+} and Mg^{2+}, the swelling and mechanical properties of $D_{AMPS/AM-SBVI}$ decreased slightly compared to NaCl solutions of equivalent concentrations. The presence of divalent ions, such as Ca^{2+} and Mg^{2+}, can interact well with the sulfonate group on AMPS or the SBVI group, making the network more compact, limiting the extent of swelling, and thereby reducing the mechanical reinforcement provided by the ionic bridges[7]. This highlights the critical role of ion specificity in the salt-responsive behavior of the hydrogel, suggesting that the ionic strength alone is not sufficient to explain the hydrogel's performance in brine. Rather, the ion-specific interactions between the hydrogel and the solution components must be considered when designing hydrogels for use in complex ionic environments.

The relevant revised section has been highlighted in yellow in the manuscript and Supporting Information.

2. ***In the abstract section, Fig. S8, the hydrogel demonstrates a 3.4-fold increase in tensile strength and a 2.1-fold enhancement in equilibrium swelling ratio in 200 g/L NaCl compared to deionized water. The authors need to specify the data that supported the 3.4-fold increase in tensile strength and 2.1-fold enhancement in equilibrium swelling ratio.***

Thank you for your careful review. We have thoroughly examined the original data and figures and found no errors in the raw measurements. However, we identified that the previous calculation method involved repetitive stacking, leading to incorrect fold-change values. We have now reviewed and revised all relevant sections throughout the manuscript. The corrected data and specific modifications are provided below:

The equilibrium swelling ratio (S_r) values of our hydrogel $D_{AMPS/AM-SBVI}$ in deionized water, 20 g/L NaCl, 100 g/L NaCl, 200 g/L NaCl, and formation brine are 17.63, 19.28, 19.74, 21.41, and 19.38, respectively, as shown in Figure R7. The water content (W_r) values of $D_{AMPS/AM-SBVI}$ in water, 20 g/L NaCl, 100 g/L NaCl, 200 g/L NaCl, and formation brine are 6.34, 6.40, 7.31, 7.88, and 7.26, respectively, as shown in Figure R8. $D_{AMPS/AM-SBVI}$ demonstrates superior swelling performance in saline solutions compared to pure water, achieving an anomalous salt-enhanced swelling property. The S_r in 200 g/L NaCl exhibits a 21.44% increase compared to that in water. The W_r in 200 g/L NaCl exhibits a 24.29% increase compared to that in water. Therefore, the correct expression is: The hydrogel demonstrates a 1.21-fold enhancement in equilibrium swelling ratio in 200 g/L NaCl compared to water.

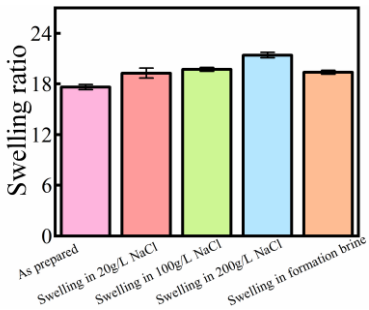

Figure R7. The swelling ratio (S_r) of hydrogels after swelling in different environments

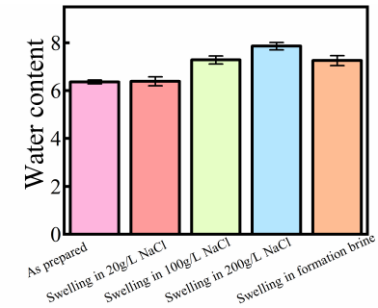

Figure R8. The water content (W_r) of hydrogels after swelling in different environments

Tensile tests of the hydrogels after reaching swelling equilibrium in different solvents are shown in Figure R9. The stress values of $D_{AMPS/AM\text{-}SBVI}$ after swelling in deionized water and 200 g/L NaCl are 0.19 MPa and 0.31 MPa, respectively. The stress in 200 g/L NaCl exhibits a 63.16% increase compared to that in water. Therefore, the correct expression is: The hydrogel demonstrates a 1.63-fold enhancement in tensile stress in 200 g/L NaCl compared to water.

The relevant revised section has been highlighted in yellow in the manuscript and Supporting Information.

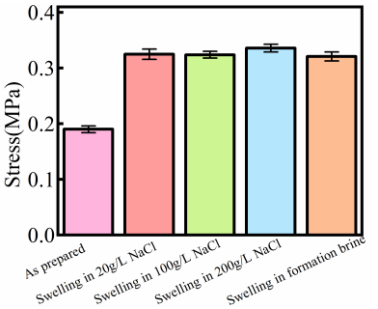

Figure R9. The stress of hydrogels after swelling in different environments

3. There are many hydrogel samples being tested as shown in the figures. The authors need to specify the feed molar ratio of monomers, feed molar ratio of first and second networks, concentration of crosslinking agents and other parameters for preparing the hydrogel samples in the figure legends.

Thank you for your careful review and suggestion. We have supplemented the relevant data of hydrogel synthesis in the figure caption in detail, as follows:

Figure 1. Design and synthesis of $D_{AMPS/AM\text{-}SBVI}$. (A) Schematic diagram of the design and fabrication of the reconfigurable salt-resistant hydrogels. (B) Fourier Transform Infrared Spectroscopy (FTIR) spectra of the S_{AMPS}, $S_{AM\text{-}SBVI}$, and

$D_{AMPS/AM-SBVI}$. (C) The optimization of the optimal molar ratio of the first network and the second network. For the first network, the AMPS, initiator and crosslinker are 0.01 M, 0.0006 M, and 0.0004 M, respectively. For the second network, the AM, SBVI, the initiator and the crosslinker are 0.1 M, 0.014 M, 0.0006 M, and 0.00061 M, respectively. The feed molar ratio of first and second network is from 1:94 to 1:27. (D) The optimization of the cross-linker concentration for the second network. For the first network, the AMPS, initiator and crosslinker are 0.01 M, 0.0006 M, and 0.0004 M, respectively. The feed molar ratio of first and second network is 1:40. For the second network, the AM, SBVI, and initiator are 0.1 M, 0.014 M, 0.0006 M, respectively. (E) The optimization of the monomer content of the second network. For the first network, the AMPS, initiator and crosslinker are are 0.01 M, 0.0006 M, and 0.0004 M, respectively. The feed molar ratio of first and second network is 1:40. For the second network, the initiator and crosslinker are 0.0006 M, and 0.00031 M respectively. The monomer ratio of AM and SBVI is 50:7. (F) The swelling ratio of SAMPS, SAM-SBVI and DAMPS/AM-SBVI after swelling brine (100 g/L NaCl). (G) The rheological properties of SAMPS, SAM-SBVI and DAMPS/AM-SBVI after swelling brine (100 g/L NaCl).

Figure S8. Systematic optimization of the monomer ratio for hydrogels. For the first network, the AMPS, initiator and crosslinker are 0.01 M, 0.0006 M, and 0.0004 M, respectively. The feed molar ratio of first and second network is 1:40. For the second network, the initiator and crosslinker are 0.0006 M, and 0.00031 M respectively. The monomer content is 0.07 M.(A) The stress-strain of the as-prepared hydrogels with different ratios. (B) The stress-strain of the water-swollen hydrogels with different ratios. (C) The stress-strain of the brine-swollen hydrogels with different ratios. (D) The toughness of water-swollen hydrogels and bine-swollen hydrogels with different ratios.

The relevant revised section has been highlighted in yellow in the manuscript and Supporting Information.

4. Line 212-215, the authors claimed that DAMPS/AM-SBVI hydrogels immersed in 200 g/L NaCl exhibit tensile stress of 0.33 MPa and strain of 123%, which are

significantly higher than those of water-swollen hydrogels (Figure 2C-E). However, based on Figure 2D, the strain of DAMPS/AM-SBVI hydrogels immersed in 200 g/L NaCl was only about 79%.

Thank you for your careful review. As addressed in our response to Question 2, we have verified that the raw data and figures contain no errors. However, the previous calculation method involved repetitive stacking, resulting in incorrect fold-change values. We have revised all relevant sections throughout the manuscript, with the corrected data and specific modifications provided below:

Tensile tests of the hydrogels after reaching swelling equilibrium in different solvents are shown in Figure R10. After swelling in deionized water, the stress and strain values of the hydrogel are 0.19 MPa and 87.76%, respectively. After swelling in 20 g/L NaCl, the stress and strain values are 0.31 MPa and 122.3%, respectively. After swelling in 100 g/L NaCl, the stress and strain values are 0.31 MPa and 100.2%, respectively. After swelling in 200 g/L NaCl, the stress and strain value are 0.31 MPa and 78.9%, respectively. After swelling in formation brine, the stress and strain value are 0.31 MPa and 91.4%, respectively. These results indicate that the stress strength of $D_{AMPS/AM\text{-}SBVI}$ after swelling in saline solutions of various concentrations is generally increased by 63.16% compared to that after swelling in water. The strain values of salt-resistant hydrogels after swelling in saline solutions are increased by up to 39.36% compared to those after swelling in deionized water.

The relevant revised section has been highlighted in yellow in the manuscript.

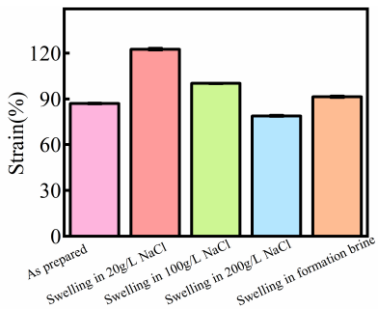

Figure R10. The strain of hydrogels after swelling in different environments

5. Based on Table S2, the molar ratio of AM in the second network is high. That said, the noncovalent interactions exerted by AM should play some role on the morphology and physical properties of the network. The formation of hydrogen

bonding, cation-dipole, and other interactions between the AM and other monomers upon salt exposure would also trigger the changes in the network morphology, swelling, and mechanical properties. This effect should be discussed and the related experiments and simulations should be conducted to elucidate the mechanism.

Thank you very much for this insightful comment.

We fully agree that the relatively high AM content in the second network should influence the morphology and physical properties of the hydrogel, and that this point needs to be discussed more carefully. Following your suggestion, we have examined the possible role of AM-related noncovalent interactions and added additional experimental and simulation analysis to clarify their contribution.

First, we would like to distinguish between (i) the contribution of AM to the baseline mechanical properties of the network and (ii) the origin of the salt-induced enhancement in swelling and mechanical performance. These two issues are related, but not identical. Because AM is present at a high molar ratio in the second network, it indeed contributes to the overall network mechanics by increasing chain entanglement, improving chain flexibility, and providing a more deformable secondary network for energy dissipation. This point is supported by our comparative rheological measurements, as shown in Figure R11 and Figure R12 . The $D_{AMPS/SBVI}$ hydrogel exhibits lower storage modulus (G′) and loss modulus (G″) than $D_{AMPS/AM-SBVI}$ after swelling in brine, confirming that AM improves the absolute mechanical level of the system.

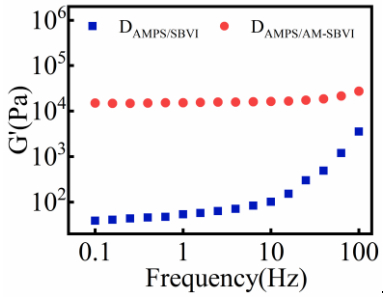

Figure R11. The G′ of $D_{AMPS/SBVI}$ and $D_{AMPS/AM-SBVI}$ after swelling in brine. $D_{AMPS/SBVI}$: The first network is AMPS and the second network is SBVI. $D_{AMPS/AM-SBVI}$: The first network is AMPS and the second network is AM and SBVI.

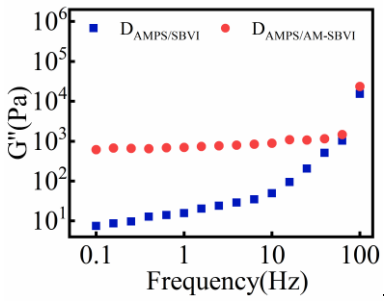

Figure R12. The G″ of $D_{AMPS/SBVI}$ and $D_{AMPS/AM-SBVI}$ after swelling in brine. $D_{AMPS/SBVI}$: The first network is AMPS and the second network is SBVI. $D_{AMPS/AM-SBVI}$: The first network is AMPS and the second network is AM and SBVI.

However, the main focus of our work is not simply why the AM-containing hydrogel is mechanically stronger in an absolute sense, but rather why the same hydrogel becomes stronger after swelling in brine than in water. In other words, our key question concerns the differential enhancement (Δ) induced by salt exposure.

To address whether AM-related noncovalent interactions dominate this salt-induced enhancement, we specifically examine these mechanisms raised by the reviewer: hydrogen bonding, cation-dipole interaction and other interactions.

For hydrogen bonding, we perform additional urea treatment experiments, since urea is widely used as a hydrogen-bond disruptor. The hydrogel samples are subjected to four conditions:

(1) Swelling in water,

(2) Swelling in brine,

(3) Swelling in urea followed by swelling in brine, and

(4) Simultaneous swelling in urea and brine.

The rheological results show that the hydrogel swollen in brine and the hydrogel swollen simultaneously in urea and brine display very similar G′ and G″. This is an important result, because if hydrogen bonding were the dominant origin of the salt-enhanced mechanical reinforcement, then disrupting hydrogen bonds in the presence of brine should have substantially weakened the modulus. However, this is not what we observe. Moreover, the sample pretreated with urea and then transferred to brine exhibits the highest G′ and G″ among the four conditions. This result further indicates that hydrogen bonding is not the principal cause of the salt-enhanced

mechanics. Instead, the removal of hydrogen-bond constraints appears to facilitate subsequent structural rearrangement in brine, thereby allowing the network to reorganize more effectively into a mechanically favorable state. Therefore, hydrogen bonding may exist in the system, but it does not account for the unusual increase in mechanical strength after salt swelling.

We also investigate the possibility of AM-related **cation-dipole interaction** under saline conditions. FTIR analysis shows that the C=O stretching vibration shifts from 1652 to 1646 cm^{-1} after swelling in brine, indicating that the carbonyl environment changes in the presence of salt. To further examine this point, we carry out DFT calculations for the interaction between Na^+ and the carbonyl oxygen of AM. The optimized structure supports the existence of a cation-dipole interaction, but the calculated binding energy is only -0.02345 eV. This value indicates that the interaction is energetically favorable yet very weak. Therefore, our interpretation is that AM-Na^+ cation-dipole interaction may exist and may assist local structural relaxation or reduce AM-rich phase association, but it is not strong enough to be regarded as the dominant load-bearing interaction or the primary driving force for the salt-enhanced mechanics. In the revised manuscript, we have therefore intentionally softened this point and now treat the cation-dipole interaction as a secondary or auxiliary effect, rather than the central mechanism. Below is the detailed discussion of the possible contributors to the hydrogel structural change under brine conditions.

1) Hydrogen binding

The noncovalent interactions encompass a wide variety, as illustrated in Figure R13, including hydrogen bonding, electrostatic interactions, hydrophobic associations, π-π stacking, coordination complex formation, and so on. Among these, hydrogen bonding has relatively strong bond energy and has been widely employed by researchers through various engineering strategies to enhance the mechanical performance of hydrogels. In high AM content systems, hydrogen bonding is the most probable noncovalent inter- and intramolecular interaction. The strengths of hydrogen bonds vary widely, ranging from weak van der Waals interactions to hydrogen bonds with moderate strength and partial covalent properties. Since the development of

cellulose dissolution method by Zhang et al. in 2004[8], urea is generally considered and used as an efficient hydrogen bond breaker between polymer chains. To verify whether hydrogen bonding triggers changes in the network mechanical properties, we employ urea (8 wt%) to disrupt hydrogen bonding in hydrogels. The experimental procedures involve subjecting hydrogels to the following treatments: (#1) swelling in water, (#2) swelling in brine, (#3) swelling in urea followed by swelling in brine, and (#4) simultaneous swelling in the swelling mixture of urea and brine. Rheological properties are then measured for each treatment group. After swelling in water (#1), the hydrogel exhibits the lowest storage modulus (G′) and loss modulus (G″), which are lower than those in brine-swollen hydrogels (#2), as shown in Figure R14 and Figure R15.

For hydrogels swollen in brine (#2) and simultaneous swelling in urea and brine (#4), the G′ and G″ are similar. This indicates that hydrogen bonding is not the key factor for mechanical enhancement, even though hydrogen bonds in the hydrogel are disrupted by urea in #4. After treatment with urea, the (#3) hydrogel exhibits the highest G′ and G″ after swelling in brine, which suggests that the disruption of hydrogen bonds by urea may create favorable conditions for the salt-enhanced mechanical property. Moreover, the storage modulus of (#3) hydrogel is almost constant when frequency increase, suggesting the hydrogel behaves like a permanent crosslinking network after urea treatment. In contrast, the storage modulus of (#2) hydrogel increases as a function of frequency, which is a typical behavior of dynamic crosslinking network. When the frequency reaches 100 Hz, the storage modulus value of (#2) hydrogel is comparable with (#3) hydrogel, suggesting the more compact and stable interaction existing in the urea treatment hydrogel. Yet, the salt induced increase in G` not only persists but is amplified, supporting a topology reinforcement rather than a hydrogen binding dominated mechanism.

We further calculate the effective crosslinking density, by G'/ζRT. The ν_e in brine is roughly 0.5 mol/m^3, and increases to 3.8 mol/m^3, 12 times rise. This is a solid support that the enhancement in mechanical properties in mainly depend on the crosslinking point increase. We do not exclude secondary contributions from

H-bonding or dipolar interactions or other interactions; however, their role is subordinate to topological conversion under the tested brine condition.

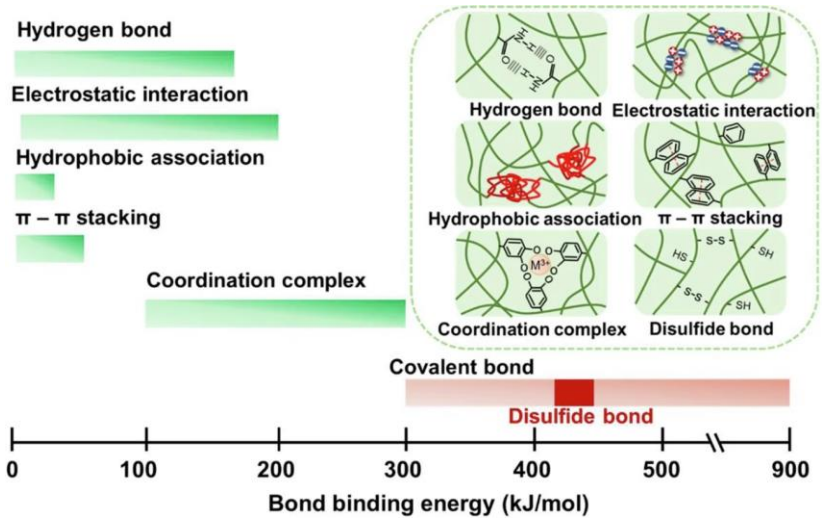

Figure R13. The binding energy of noncovalent interactions[9].

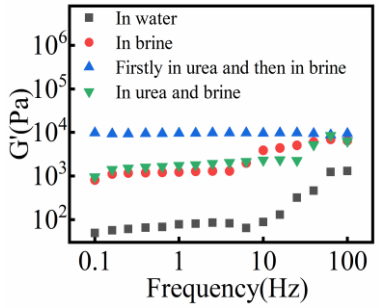

Figure R14. The storage modulus (G′) of hydrogels with different treatments.

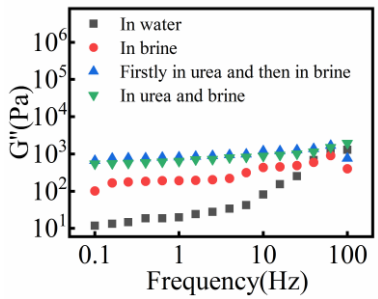

Figure R15. The loss modulus (G″) of hydrogels with different treatments.

2) Ion-dipole interaction

As you correctly pointed out, in a saline environment, AM may form ion-dipole interactions with ions. Ion-dipole interaction, specifically the electrostatic attraction between cations and polar molecules, has been recognized as one of the most effective approaches for enhancing ionic conductivity in ion exchange membranes[10]. This mechanism has been widely exploited to improve ion transport in hydrogels by

creating abundant pores or channels within the polymer network. In our system, SEM images reveal distinct morphological differences between hydrogels swollen in water and brine. The water-swollen hydrogel displayed a heterogeneous polymer matrix with constricted pores and reduced porosity, typical of phase-separated structures, as shown in Figure R16. In contrast, the brine-swollen hydrogel exhibited a more homogeneous structure, characterized by expanded pores and a looser network topology. We initially attribute this morphological change to the ability of salt ions to disrupt phase separation and induce structural adaptation. Inspired by the ion-dipole interaction mechanism reported in ion exchange membranes, we propose that Na^+ coordinates with the carbonyl oxygen of AM through cation-dipole interactions, promoting the formation of a more porous and homogeneous network.

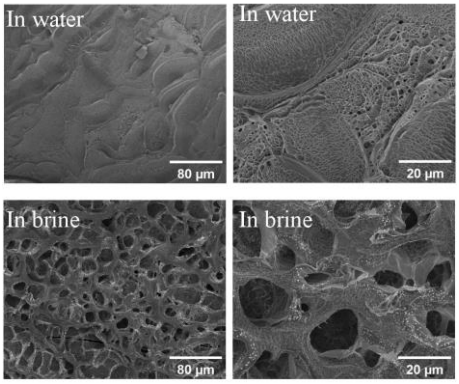

Figure R16. The SEM images of hydrogels swelling in different solutions.

To gain deeper insight into this mechanism, we perform FTIR analyses of hydrogels $D_{AMPS/SBVI}$ and $D_{AMPS/AM\text{-}SBVI}$. As shown in Figure R17, the FTIR results show a shift in the C=O stretching vibration from 1652 to 1646 cm^{-1}, indicating a changed carbonyl environment and a reduced C=O bond force constant. This red shift suggests strengthened intermolecular interactions involving the carbonyl groups, which may include ionic coordination.

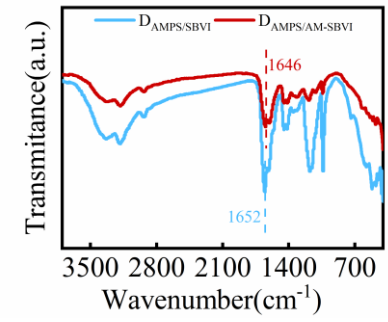

Figure R17. The FTIR of $D_{AMPS/SBVI}$ and $D_{AMPS/AM-SBVI}$ swelling in 100 g/L NaCl. $D_{AMPS/SBVI}$: The first network is AMPS and the second network is SBVI. $D_{AMPS/AM-SBVI}$: The first network is AMPS and the second network is AM and SBVI.

To further validate the cation-dipole interaction between AM and Na^+, density functional theory (DFT) calculations are performed using the B3LYP functional. The optimized geometry and electrostatic potential distribution revealed that Na^+ interacts with the carbonyl oxygen of AM through electrostatic attraction (cation-dipole interaction), as shown in Figure R18.

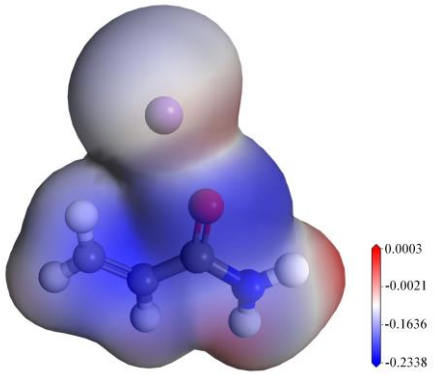

Figure R18. The electrostatic potential distribution of AM and Na^+

The binding energy is calculated as $E_{binding\ energy} = E_{(AM\text{-}Na+)} - E_{(AM)} - E_{(Na+)}$. The binding energy of O-Na^+ is calculated to be -0.02345 eV, indicating an energetically favorable but weak interaction between Na^+ and carbonyl oxygen. Based on these findings, the ion-dipole interactions disrupt the phase-separated structure, leading to the observed morphological changes and contributing the swelling property.

3) For other interactions:

Beyond hydrogen bonding and cation-dipole interaction, we also agree that other AM-related weak interactions may exist after salt exposure. In the present hydrogel system, these are more reasonably understood as nonspecific amide-amide dipole association, weak van der Waals contacts, salt-modulated local aggregation, and entanglement-assisted local rearrangement within the AM-containing second network. Such interactions may influence local morphology, chain entanglement, and the baseline viscoelastic response of the hydrogel. However, based on the currently available evidence, we do not consider these AM-related interactions to be the dominant origin of the salt-enhanced changes in morphology, swelling, and

mechanical performance. Instead, they are more appropriately regarded as supplemental contributors to accompany local structural adaptation, whereas the primary mechanism remains the salt-triggered topological conversion of SBVI-based intrachain loops into inter-network reversible bridges with AMPS.

Based on these additional results, our conclusion is as follows. The high AM content does affect the network morphology and the baseline physical properties of the hydrogel. AM improves the deformability and entanglement of the second network, and weak AM-related noncovalent interactions may participate in local rearrangement under saline conditions. However, these AM-centered interactions do not primarily govern the salt-induced enhancement in swelling and mechanical strength. The dominant mechanism remains the salt-triggered topological reconfiguration of the network: salt screens the intrachain zwitterionic ion-pair loops associated with SBVI, exposes additional ionic sites, and promotes their reorganization into inter-network reversible bridges with AMPS. This loop-to-bridge conversion decreases the fraction of non-load-bearing loops and increases the effective load-bearing connectivity of the swollen network, thereby explaining why the hydrogel becomes simultaneously more swollen and mechanically stronger in brine.

To avoid misunderstanding, we have revised the manuscript and Supporting Information to clarify the hierarchy of contributions more explicitly following:

(1) AM contributes to the baseline mechanical robustness of the second network;

(2) Hydrogen bonding is not the dominant source of the salt-enhanced reinforcement;

(3) AM-related cation-dipole interaction may exist, but it is weak and auxiliary;

(4) The principal origin of the anomalous salt-enhanced behavior is the salt-induced topological conversion of SBVI-based intrachain loops into inter-network $SBVI^{+}$-$AMPS^{-}$ bridges.

The relevant revised section has been highlighted in yellow in the manuscript and Supporting Information.

6. The enhancement of both hydrogel mechanical strength and swelling

performance is very complex. The authors mainly attributed it to a stronger interaction between SBVI and AMPS under high salinity water simply based on the simulation calculation. There might be several mechanisms that contributed to the enhancement. For example, it is possible that, upon salt exposure, the hydrogen bonding, cation-dipole, and other interactions between the AM and other monomers were screened and triggered the rearrangement of polymeric network and increase of ionic/nonionic bridging, partly contributing to network stability and salt-enhanced elasticity.

Thank you very much for this insightful and important comment. We fully agree that the simultaneous enhancement of swelling and mechanical properties in brine is a complex and multifactorial process, and should not be interpreted as the consequence of a single interaction or a single simulation result. We have therefore carefully revised our discussion to clarify the hierarchy of contributions and to avoid over-attributing the observed behavior to one isolated factor.

First, we would like to clarify that our mechanistic conclusion is not based solely on the simulation result of stronger SBVI-AMPS interaction under high salinity conditions. Rather, our interpretation is derived from the combined evidence of swelling behavior, rheology, SAXS/XPS characterization, hydrogen-bond perturbation experiments, FTIR/DFT analysis, and thermodynamic/free-energy analysis. In the revised manuscript, we now emphasize that the unusual co-enhancement arises from a network-level topological reconfiguration, while AM-related local interactions may participate as secondary contributors. This clarification is important because the key phenomenon in our system is not simply a higher modulus, but the fact that the hydrogel becomes more swollen and simultaneously mechanically stronger in brine than in water, which is opposite to the classical swelling-strength trade-off expected from Flory-Rehner and rubber elasticity arguments.

Based on the swelling and rheology data across five aqueous media, we extract three descriptors of the swollen network, namely the effective bridge density (ν_e), the effective solvent parameter (χ), and the absolute loop fraction (f_{loop}), and then resolve

the free-energy density into four contributions, $F_{tot} = F_{mix} + F_{el} + F_{ion} + F_{assoc}$. The results show that ν_e increases strongly with salt concentration, while f_{loop} decreases monotonically from 0.55 in water to 0.14 in 100 g/L NaCl, indicating progressive conversion of non-load-bearing intrachain loops into load-bearing bridges. In parallel, the free-energy decomposition shows that the principal balance is between the increasing elastic penalty (F_{el}) and the increasingly favorable associative stabilization (F_{assoc}), whereas F_{ion} is much smaller and F_{mix} changes only modestly. These results directly support a salt-induced loop-to-bridge topological conversion as the main structural origin of the co-enhanced swelling and modulus. In other words, the coexistence of larger swelling and higher modulus does not arise from a better solvent environment alone, but from salt-driven topology control that increases effective load-bearing connectivity in the swollen state.

At the same time, we agree with the reviewer that AM-related noncovalent interactions may also participate in this process, and we have now addressed this point more carefully.

1) Hydrogen bonding

With respect to hydrogen bonding, we carry out additional urea-treatment experiments, since urea is a widely used hydrogen-bond disruptor. Four conditions are compared: swelling in water, swelling in brine, swelling in urea followed by swelling in brine, and simultaneous swelling in urea and brine. The rheological results show that the hydrogel swollen in brine and the hydrogel swollen simultaneously in urea and brine display similar G' and G", indicating that disruption of hydrogen bonding does not eliminate the salt-enhanced mechanical response. Moreover, the hydrogel pretreated with urea and subsequently swollen in brine exhibits the highest G' and G" among all groups. These observations indicate that hydrogen bonding is not the dominant source of the mechanical enhancement after salt swelling. Instead, disrupting hydrogen-bond constraints appears to facilitate later structural reorganization in brine. Therefore, hydrogen bonding may affect local chain conformation, but it cannot account for the anomalous co-enhancement observed in saline media.

2) Caion-dipole interaction

With respect to cation-dipole interaction, we agree that AM may interact with salt ions under brine conditions. FTIR analysis shows that the C=O stretching band shifts from 1652 to 1646 cm^{-1} after swelling in brine, indicating that the carbonyl environment changes in saline solution. To further probe this possibility, we performed DFT calculations for the interaction between Na^+ and the carbonyl oxygen of AM. The calculation supports the existence of an AM-Na^+ cation-dipole interaction, but the calculated binding energy is only -0.02345 eV, indicating that this interaction is energetically favorable yet weak. We therefore interpret this interaction cautiously: it may assist local chain relaxation and structural adaptation, but it is not sufficiently strong to be considered the principal load-bearing interaction or the dominant driving force for the salt-enhanced mechanics and swelling.

3) Other interactions

Beyond hydrogen bonding and cation-dipole interaction, we also agree with the reviewer that other AM-related weak interactions may exist after salt exposure. In the present system, these are more reasonably understood as nonspecific amide-amide dipole-dipole association, weak van der Waals contacts, salt-modulated local aggregation, and physical entanglement-assisted structural relaxation within the AM-containing second network, rather than as strong, well-defined directional bonds. Such effects may influence local morphology, chain packing, and baseline viscoelasticity of the hydrogel. However, based on the currently available evidence, we do not consider these AM-related interactions to be the dominant origin of the anomalous salt-enhanced co-improvement in swelling and mechanical strength. This conclusion is based on our new experiment results: 1) the strongest plausible AM-related directional interaction, hydrogen bonding, can be disrupted without eliminating the salt-enhanced mechanics; 2) the directly probed AM-Na^+ cation-dipole interaction is weak in energy; 3) the strongest quantitative evidence from our system points instead to increased ν_e, decreased f_{loop}, and the F_{el}/F_{assoc} trade-off characteristic of loop-to-bridge conversion. Accordingly, these weak AM-related interactions are better regarded as secondary contributors that accompany local structural adaptation,

rather than as the dominant mechanism that drives the macroscopic salt-enhanced elasticity.

Therefore, we revise our paper as we fully agree that there are many factors affect the enhancement process, which we have state that in the revised manuscript version. For AM-related interactions, hydrogen bonding, weak cation-dipole interaction, and other nonspecific local associations may participate in morphological adjustment and structural relaxation under saline conditions. However, the currently available experiments and calculations do not support these AM-centered interactions as the dominant origin of the unusual co-enhancement. The dominant mechanism is the salt-induced topological reconfiguration of the double-network hydrogel: salt screens SBVI-based intrachain ionic loops, exposes ionic sites, and promotes their reorganization into inter-network reversible $SBVI^{+}$-$AMPS^{-}$ bridges. This conversion decreases the fraction of non-load-bearing loops and increases the effective load-bearing connectivity of the swollen network, thereby enabling simultaneous enhancement of swelling and mechanical strength in brine.

To avoid misunderstanding, we have revised the manuscript and Supporting Information accordingly, and highlighted in yellow. In the revised version, we no longer present AM-related cation-dipole interaction or other AM-centered weak interactions as the responsible factor for the overall enhancement. Instead, they are now described as possible auxiliary effects, whereas the primary mechanism is the salt-triggered loop-to-bridge topological conversion within the double-network hydrogel system, as shown in Figure R19.

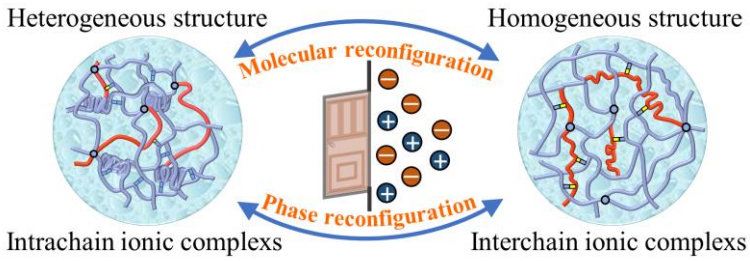

Figure R19. Schematic illustration of structural evolution of the hydrogel in brine

Reviewer #2 (Remarks to the Author):

This manuscript reports a double-network hydrogel composed of poly(AMPS)

and poly(SBVI-co-Am) networks, which exhibits salt-enhanced mechanical properties. While the mechanical performance and structure of the gel are investigated, several critical issues must be addressed before the work can be considered for publication.

1. The introduction section is rather confusing. Whether for zwitterionic polymers or other types of polymers, most undergo changes in network structure and mechanical properties in saline environments. The authors have not adequately categorized or elaborated on these aspects. Moreover, when reading these paragraphs, it is difficult to discern the authors' intention: Is the goal to obtain gels with unchanged mechanical properties in brine, or to develop gels with enhanced performance in brine? If the latter, there have already been numerous reports of ion-enhanced cases in various polymer systems, including single-charged polymers, zwitterionic polymers, and non-ionic polymers. Therefore, the authors need to highlight the innovation and uniqueness of this work.

Thank the reviewer for this constructive and important comment.

We agree that the original ***Introduction*** does not sufficiently distinguish among different classes of salt-responsive polymer systems, nor does it clearly state the specific objective and novelty of this work. The earlier version does not adequately separate the broader problem of maintaining hydrogel stability in saline environments from the specific question addressed here, namely, how to design a hydrogel that exhibits simultaneous enhancement of swelling and mechanical performance in brine. Therefore, we have substantially revised the Introduction to clarify both the research context and the innovation of the present study.

In the revised Introduction, we first define the general challenge of hydrogel instability under high-ionic-strength conditions, emphasizing that cation-mediated screening and reduced polymer-solvent affinity commonly lead to dehydration, collapse, and weakened load-bearing connectivity. Then, we reorganize the literature discussion by distinguishing among charged polymer systems, zwitterionic polymer systems, and nonionic polymer systems, and clarify the typical saline responses and limitations of each class. This revision is intended to provide a clearer framework for readers and to position our work more precisely within the broader field.

We also explicitly clarify our objective. The purpose of this work is not to obtain a hydrogel whose swelling and mechanical properties remain unchanged in brine relative to water. Rather, our purpose is to understand and how the principle of a system with more swollen and mechanically stronger under high-salinity conditions at the same time. We agree with the reviewer that cation-enhanced behavior has been reported in various works. Accordingly, in the revised Introduction, we no longer present our work simply as another example of salt-enhanced performance. Instead, we highlight that the key innovation of this study lies in the quantitative mechanistic resolution of this co-enhancement. Specifically, we now emphasize that the central contribution of this work is the identification of a salt-triggered topological reconfiguration mechanism in the $D_{AMPS/AM\text{-}SBVI}$ double-network hydrogel. To quantify this process, we introduce three experimentally descriptors, effective bridge density (ν_e), effective Flory-Huggins parameter (χ), and absolute loop fraction (f_{loop}), and further resolve the free energy into mixing, elastic, associative, and ionic contributions. This framework allows us to explain why our hydrogel does not merely resist saline deterioration, but instead undergoes a structural adaptation in which swelling is coupled to an increase in effective load-bearing connectivity. We believe this distinguishes the present work from prior studies that primarily reported phenomenological salt responsiveness or property enhancement without resolving the underlying network-level mechanism.

For summarized, the Introduction has been substantially rewritten to: (1) categorize the relevant saline-responsive hydrogel systems more clearly; (2) distinguish our target of simultaneous swelling and mechanical enhancement in brine from the broader goal of saline stability; (3) highlight the uniqueness of this study as a quantitative mechanistic analysis of cation-triggered topological adaptation, rather than simply another double-network or cation-enhanced hydrogel example. Below is our revise version, and we also highlight in yellow in the manuscript.

Hydrogels are water-swollen polymer networks with tunable hydration, transport, and mechanical properties, making them attractive for applications ranging from water treatment [11, 12]and enhanced oil recovery (EOR)[13, 14] to implantable biomedical

devices[15, 16]. Yet under high-ionic-strength conditions, conventional hydrogels commonly undergo dehydration, loss of swelling capacity, and mechanical deterioration[17, 18, 19]. This instability arises primarily from ion-mediated screening of charged segments and the concomitant reduction in effective polymer-solvent affinity[20, 21], which disrupts hydration, alters chain conformation and mesh structure, and diminishes load-bearing network connectivity[22, 23].

From a thermodynamic perspective, this behavior is classically described by Flory-Rehner theory, in which equilibrium swelling is governed by the balance between mixing and elastic free energies[24, 25]. In brine, hydrated ions weaken polymer-solvent interactions and suppress electrostatic contributions to swelling[26, 27], often driving excessive shrinkage, structural collapse, or uncontrolled deformation, particularly in networks with high ionic content or limited cohesive stabilization[28]. Substantial effort has therefore been devoted to improving hydrogel performance in saline environments. Increasing the density of ionic groups can enhance hydration under moderate salinity[29, 30, 31]; however at higher salt concentrations, this strategy may intensify ion-water competition and accelerate charge screening. Zwitterionic polymers provide an important alternative because their strong hydration and internal charge neutrality can produce anti-polyelectrolyte behavior[32, 33]. However, many zwitterionic hydrogels still show either mechanical softening or collapse of dynamic ionic associations in salt-rich media[34], so that swelling and mechanical robustness cannot be improved simultaneously. Nonionic networks are less directly affected by electrostatic screening, but they often remain limited by reduced solvent quality, phase separation, or insufficient adaptability under concentrated brine[35, 36]. More broadly, although salt-responsive and ion-enhanced behaviors have been reported in charged, zwitterionic, and nonionic polymer systems, current studies have focused on preserving structural integrity or improving a single property in saline environments [37, 38, 39]. By contrast, hydrogels that become both more swollen and mechanically stronger in concentrated brine remain comparatively rare, and the molecular basis of this co-enhancement has not been quantitatively resolved. This problem is fundamentally challenging because swelling and stiffness are ordinarily coupled in

opposite directions. Rubber elasticity relates mechanical stiffness to the density of load-bearing network connections, whereas swelling lowers the polymer volume fraction and generally dilutes effective connectivity. Accordingly, conventional theory predicts that stronger swelling should be accompanied by weaker mechanics unless the network reorganizes to generate new mechanically effective junctions during swelling. The central question of this work is therefore not how to maintain hydrogel properties in brine relative to water, but how to design a saline-responsive network that undergoes structural adaptation such that swelling is coupled to an increase in load-bearing connectivity rather than to its loss.

Here, we report a double-network hydrogel, denoted $D_{AMPS/AM\text{-}SBVI}$, that exhibits simultaneous enhancement of swelling and mechanical performance under high-salinity conditions compared to that in water. The first network is poly(2-acrylamido-2-methylpropane sulfonic acid) (poly(AMPS)), while the second network is composed of acrylamide (AM) and a newly synthesized zwitterionic monomer, sulfobetaine vinylimidazole (SBVI). We show that salt exposure induces a topological reconfiguration of the swollen network, in which zwitterionic intrachain ion-pair loops are disrupted and reorganized into reversible load-bearing bridges between the two networks. To quantify this process, we introduce three experimentally accessible descriptors: the effective bridge density (ν_e), the effective Flory-Huggins parameter (χ), and the absolute loop fraction (f_{loop}). We further resolve the free energy into mixing (F_{mix}), elastic (F_{el}), associative (F_{assoc}), and ionic (F_{ion}) contributions to define the energetic basis of the saline response. SAXS, XPS, and DFT analyses reveal the associated structural rearrangement and charge redistribution, while core-flooding experiments demonstrate the utility of this hydrogel in high-salinity porous media. Together, these results establish a quantitative framework for understanding how ion-triggered topological adaptation converts swelling into mechanically effective connectivity and provide a design principle for hydrogels required to operate in harsh saline environments.

2. There are many zwitterionic monomers, the reason for choosing SBVI should be clarified properly. It is very important to illustrate the design method of

materials.

Thank you for this valuable comment. We totally agree that the rationale for selecting SBVI should be clarified. The following is our rationale for selecting SBVI：

Zwitterionic monomers are functional polymers containing equal amounts of positively and negatively charged groups, which can associate through electrostatic interactions. When salt ions are present, the electrostatic interactions are weakened or even dissociated, causing the hydrogel to swell and become softer, thereby exhibiting salt-responsive property. The salt responsiveness of zwitterionic polymers originates from the destruction and reconstruction of intermolecular interactions. Therefore, the zwitterionic unit structure directly affects its stimuli-responsive behavior.

The zwitterionic monomers commonly used in existing research can be mainly divided into three categories: (1) carboxybetaines consisting of quaternary ammonium cations and carboxylate anions, such as 3-((2-(methacryloyloxy)ethyl) dimethylammonio) propionate (CBMA); (2) sulfobetaine monomers consisting of quaternary ammonium cations and sulfonate anions, such as 3-(N,N-dimethyl-(2-(2-methylprop-2-enoyloxy)ethyl)ammonio) propane-1-sulfonate (SBMA); (3) phosphorylcholine monomers consisting of quaternary ammonium cations and phosphate anions, such as 2-(methacryloyloxy)ethyl phosphorylcholine (MPC)[40]. Among these, carboxybetaine and sulfobetaine have been most widely studied. Carboxybetaine has lower hydration free energy in water, which preferentially binds to water molecules rather than forming electrostatic interactions between carboxybetaine groups. This results in weak self-association and conventional carboxybetaine hydrogels almost exhibit no salt responsiveness[41]. In contrast, sulfobetaine has a weaker water-binding ability compared to carboxybetaine, leading to more significant self-association and a pronounced anti-polyelectrolyte effect. Therefore, sulfobetaine is preferred for hydrogel design requiring salt responsiveness.

Furthermore, the anti-polyelectrolyte effect of sulfobetaine can be further enhanced through two approaches: (1) strengthening physical interactions between zwitterionic polymer chains by introducing highly folded network structures, such as

incorporating benzene rings or imidazolium cation structures[34]; (2) strengthening the interaction between zwitterionic units and salt ions to promote dissociation of inter-chain electrostatic interactions. For instance, higher-valency cation salts (e.g., Ca^{2+}) can form stronger interactions with zwitterionic polymers compared to monovalent cation salts (e.g., Na^{+}), resulting in more significant anti-polyelectrolyte effects[42].

In this study, we select SBVI (a copolymer of propanesultone and vinyl imidazole, i.e., sulfobetaine vinyl imidazole) as the zwitterionic monomer, which is a sulfobetaine monomer containing an imidazolium cation structure. This design combines the advantages of sulfobetaine's inherent anti-polyelectrolyte effect with the enhanced physical interactions provided by the imidazolium cation. This is validated by experimental comparisons with $D_{AMPS\text{-}SBVI}$ and $D_{AMPS\text{-}SBMA}$ hydrogels. In the $D_{AMPS\text{-}SBVI}$ system, the first network AMPS is synthesized and fully swollen in a predetermined amount of SBVI solution prior to polymerization. Similarly, in the $D_{AMPS\text{-}SBMA}$ system, the first network AMPS is synthesized and fully swollen in a predetermined amount of SBMA solution prior to polymerization. As shown in Figure R20, the $D_{AMPS\text{-}SBVI}$ hydrogel appears opaque in water due to strong inter-chain associations, whereas the $D_{AMPS\text{-}SBMA}$ hydrogel becomes transparent after swelling, indicating weaker self-association. Additionally, $D_{AMPS\text{-}SBVI}$ exhibits superior mechanical properties, with both storage modulus (G′) and loss modulus (G″)higher than those of $D_{AMPS\text{-}SBMA}$ (Figure R21). These advantages make SBVI an optimal choice for constructing salt-responsive hydrogels with enhanced mechanical performance.

The relevant revised section has been highlighted in yellow in the manuscript and Supporting Information.

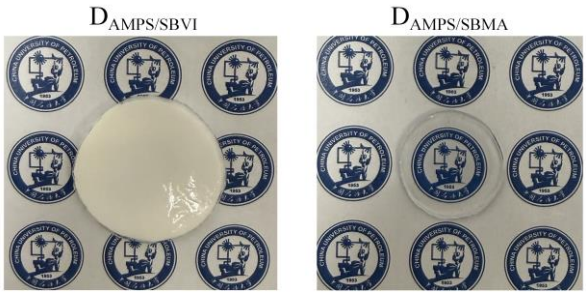

Figure R20. Morphological images of $D_{AMPS\text{-}SBVI}$ and $D_{AMPS/SBMA}$ hydrogels after swelling in water. $D_{AMPS/SBVI}$: The first network is AMPS and the second network is SBVI. $D_{AMPS/SBMA}$: The first network is AMPS and the second network is SBMA.

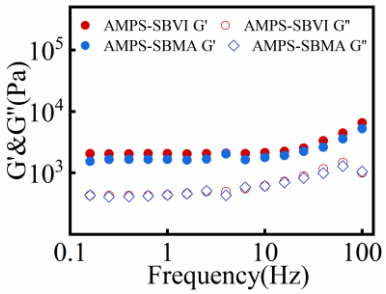

Figure R21. Rheological properties of $D_{AMPS\text{-}SBVI}$ and $D_{AMPS/SBMA}$ hydrogels after swelling in water. $D_{AMPS/SBVI}$: The first network is AMPS and the second network is SBVI. $D_{AMPS/SBMA}$: The first network is AMPS and the second network is SBMA.

3. In the text, the abbreviation appeared first time should have its full name. For example, the "EOR" at line 71, page 4.

Thank you for your careful review and suggestion. We have revised the manuscript to include the full name "Enhanced Oil Recovery (EOR)" at its first occurrence. We have also double-checked all other abbreviations throughout the manuscript to ensure they are properly defined.

The relevant revised section has been highlighted in yellow in the manuscript.

4. The shape of the tensile stress-strain curve appears unusual, as a plateau is observed in the later stage of stretching. This differs from the typical behavior of glass materials, elastomers, and gels. Could this be due to the gel sample gradually slipping from the grips of the tensile machine? The authors need to provide an explanation for this phenomenon.

Thank you for your careful review and insightful question regarding the unusual plateau observed in the tensile stress-strain curve.

We have conducted systematic control experiments and analysis to address this

concern. First, to rule out the possibility of grip slipping during the tensile test, we mark the specimen at the grip boundaries before each test and examined the relative position after stretching, as shown in Figure R22. The results show that the marked positions remained aligned with the grips before and after stretching. In addition, Video 1 shows no obvious relative displacement between the specimen and the grips during stretching. Therefore, the plateau cannot be attributed to grip slippage.

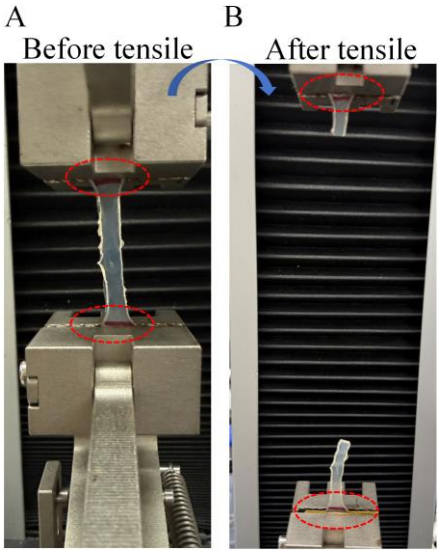

Figure R22. Schematic diagram of grip's position before and after gel stretching

We found that the appearance of the plateau is closely related to the content of the second network. The plateau only appears when the second network monomer content exceeds 1:67, as shown Figure R23, where no obvious plateau is observed in samples with lower second network content. This indicates that the plateau is structurally associated with the second network architecture rather than arising from a testing artifact.

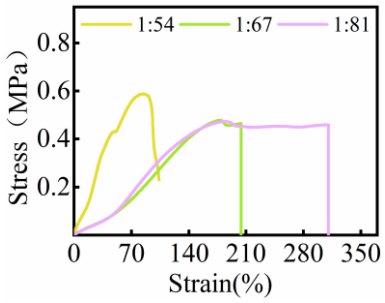

Figure R23. The tensile stress-strain curve of hydrogels

Direct observation of the stretching process shows that the deformation can be divided into three stages, as shown in Figure R24. In Stage I, the sample deforms

approximately elastically and the stress increases with strain, as shown in Figure R25 A. In Stage II, localized damage initiates, as indicated by the appearance of a small crack and slight stress softening. This stage corresponds to the onset of fracture of the brittle first network, which serves as a sacrificial network for energy dissipation, as shown in Figure R25 B. In Stage III, the hydrogel undergoes pronounced necking, and the necked region gradually propagates while the stress remains nearly constant, as shown in Figure R25 C. During this stage, the loosely crosslinked and highly entangled second network remains intact and continues to bear the load through chain sliding, alignment, and progressive thinning, thereby producing the plateau in the stress-strain curve.

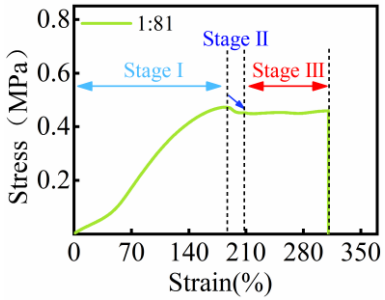

Figure R24. The tensile stress-strain curve of the hydrogel

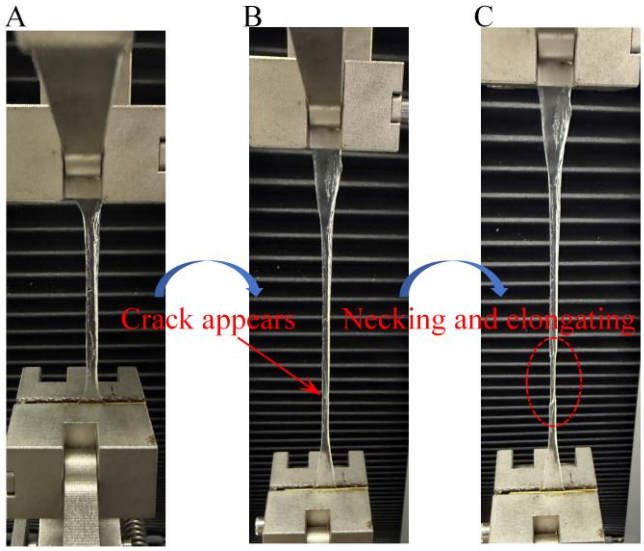

Figure R25. Morphological changes of the gel during stretching process: (A) initial stretching, (B) crack initiation, (C) gradual necking and elongation

Based on the double network (DN) hydrogel design principle, the observed three-stage deformation can be explained. In our experimental system, the first network is designed with high crosslinking density, making it stiff and brittle. The

second network follows a design principle of low crosslinker content and high monomer content, thereby increasing the degree of chain entanglements and improving the toughness of the hydrogel. Specifically, in Stage I, both networks deform elastically together. In Stage II, the high-crosslinking-density first network reaches its critical stress (0.45 MPa) and begins to fracture, forming small cracks and causing slight stress softening. This is consistent with the principle that the stiff first network ruptures preferentially. At this point, the first network serves as a sacrificial bond that breaks to dissipate energy, while the second network with high chain entanglements remains intact and continues to bear the load. In Stage III, the second network, characterized by low crosslinker content and high chain entanglements, maintains the constant stress. Under sustained loading, the entangled chains gradually slide and align along the stretching direction, leading to significant necking and thinning of the gel. The hydrogel continues to elongate under constant stress, forming a distinct plateau in the stress-strain curve. This is consistent with the plateau phenomena reported in entanglement-dominated hydrogel systems[43, 44]. We have performed multiple repeated experiments on the groups exhibiting the plateau, and the results demonstrate good reproducibility. These findings indicate that the plateau originates from the sustained load-bearing mechanism of the highly entangled second network after the first network fracture, representing an intrinsic behavior of the material rather than an experimental artifact. Therefore, this behavior is not interpreted as grip slippage or another experimental artifact, but as an intrinsic yielding or necking response of the double-network hydrogel. Such a plateau-like regime has been reported in necking-dominated or entanglement-dominated DN hydrogel systems, where stress remains nearly constant during neck propagation. Repeated measurements of the plateau-containing samples also show good reproducibility, further supporting this interpretation.

The relevant revised section has been highlighted in yellow in the manuscript and Supporting Information.

5. The Young's modulus of the gels with varying conditions should be calculated and compared, which was associated with cross-linking density of the

network. Besides, it is also suggest to compare Young's modulus with shear modulus.

Thank you for this valuable suggestion. According to your suggestion, we calculate the Young's modulus of the hydrogels swollen in different conditions from the slope of the linear region (strain range: 10-20%) of the stress-strain curve. As shown in Figure R26, the Young's modulus of hydrogels swollen in water, 20 g/L NaCl, 100 g/L NaCl, 200 g/L NaCl, and formation brine are 608.32 Pa, 3321.86 Pa, 5084.69 Pa, 6509.25 Pa, and 6121.68 Pa, respectively. These results show that the tensile stiffness is substantially enhanced after swelling in saline media relative to water, which is consistent with the salt-strengthening behavior observed in the tensile tests.

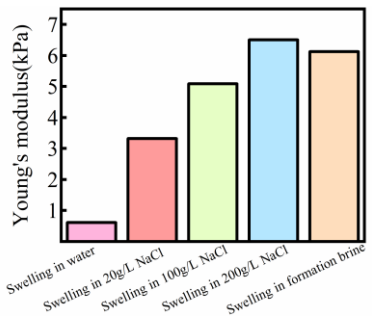

Figure R26. The Young's modulus of hydrogels swollen in different solutions

We also compare the Young's modulus with the shear modulus obtained from rheological measurements, as shown in Figure R27 to Figure R30. The shear modulus is determined from dynamic strain sweep tests by identifying the linear viscoelastic region (LVR), in which the storage modulus G′ remains essentially constant; the shear modulus is then calculated by averaging the G′ values within the LVR. The corresponding shear modulus values for hydrogels swollen in water, 20 g/L NaCl, 100 g/L NaCl, 200 g/L NaCl, and formation brine are 78.12 Pa, 251.47 Pa, 305.53 Pa, 127.48 Pa, and 253.69 Pa, respectively. We would like to emphasize that the Young's modulus and shear modulus are obtained from different deformation modes and measurement conditions. The Young's modulus is extracted from uniaxial tensile deformation, whereas the shear modulus is obtained from small-amplitude oscillatory shear deformation. So, these two quantities should not be expected to show direct numerical equivalence. Instead, they provide complementary information on the

mechanical response of the hydrogel network under tensile and shear deformation, respectively.

Although the detailed salt dependence is not identical for the two moduli, both measurements show that the hydrogel becomes mechanically stiffer in saline environments than in water. In particular, Young's modulus increases markedly with salinity, while the shear modulus also increases substantially from water to saline conditions, with the maximum value observed at 100 g/L NaCl under oscillatory shear mode. This difference likely reflects the viscoelastic and deformation-mode-dependent response of the swollen double-network hydrogel, rather than inconsistency in the measurements. Thus, the combined tensile and rheological results consistently support salt-enhanced network reinforcement.

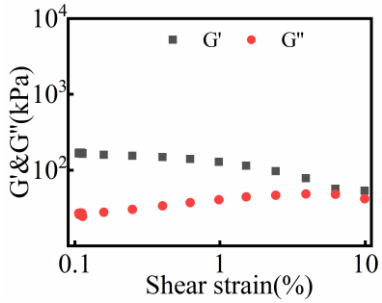

Figure R27. Strain sweep measurement of hydrogel swollen in 20 g/L NaCl.

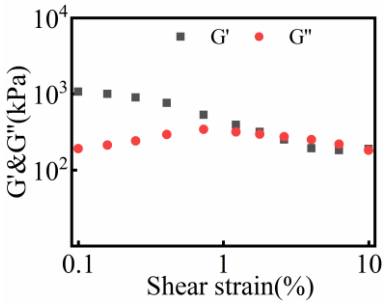

Figure R28. Strain sweep measurement of hydrogel swollen in 100g/L NaCl.

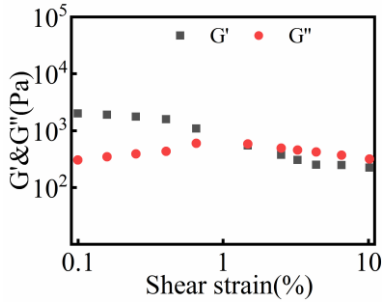

Figure R29. Strain sweep measurement of hydrogel swollen in 200g/L NaCl.

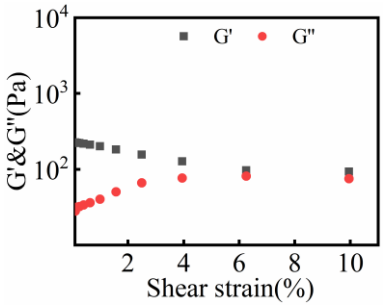

Figure R30. Strain sweep measurement of hydrogel swollen in formation brine.

To further quantify these mechanical results with network structure, we calculate the effective cross-linking density (ν_e) based on the small-strain modulus G' using the theory of rubber elasticity.

$$\nu_e = \frac{G'}{\zeta RT}$$

ζ is the phantom network model correction factor with a value of 1 unless noted. As shown in the revised manuscript, ν_e increases from 2.54 to 5.71 mol/m^3 with increasing NaCl concentration, indicating that the salt exposure increases the effective load-bearing connectivity of the network. Therefore, rather than attributing the mechanical enhancement simply to a high permanent crosslinking density, we interpret it more precisely as a salt-induced increase in effective network connectivity density.

The relevant revised section has been highlighted in yellow in the manuscript and Supporting Information.

6. In Figure 1G, the comparison with single-network samples that equilibrated in water is of limited significance, as the effectiveness of the double-network in enhancing the toughness of hydrogels has already been well-established through repeated demonstrations after 2003. Instead, to clarify the key mechanism of this work, the mechanical performance, structural changes, and swelling behavior of each single-network gel component in saline water should be examined and thoroughly compared.

Thank you for this constructive suggestion.

We agree that the original comparison in Figure 1G did not directly address the key mechanistic question raised by this work. As you correctly pointed out, the

superiority of double-network hydrogels over single-network hydrogels in terms of toughness has already been well-established by Jianping Gong in 2003. In fact, we do not intend to demonstrate this well-known advantage again and we aim to emphasize the mechanical and salt-resistant benefits brought by the synergistic effect of the two networks, which is the key innovation of our study. Following your suggestion, we expand the comparison to include single-network AMPS hydrogel (S_{AMPS}), single-network AM and SBVI hydrogel ($S_{AM\text{-}SBVI}$) and double-network hydrogel $D_{AMPS/,AM\text{-}SBVI}$, and systematically examine their morphology, swelling behavior, and mechanical properties in brine(100 g/L NaCl).

The hydrogels are immersed in water and brine (100 g/L NaCl), respectively, to observe their morphological changes. S_{AMPS} remains fully transparent in both water and saline, as shown in Figure R31. $S_{AM\text{-}SBVI}$ shows slight opacity in water but becomes transparent in saline. $S_{AM\text{-}SBVI}$ exhibits partial anti-polyelectrolyte behavior. $D_{AMPS/AM\text{-}SBVI}$ is opaque in water but transparent in saline. Notably, this transparency transition is reversible. When transferred back to water, $D_{AMPS/AM\text{-}SBVI}$ turns opaque again, as shown in Figure R32. The transparency changes arise from variations in refractive index caused by electrostatic interaction-induced phase separation. These results indicate that the salt-triggered structural reorganization is much more pronounced in the double network architecture than in either single network control.

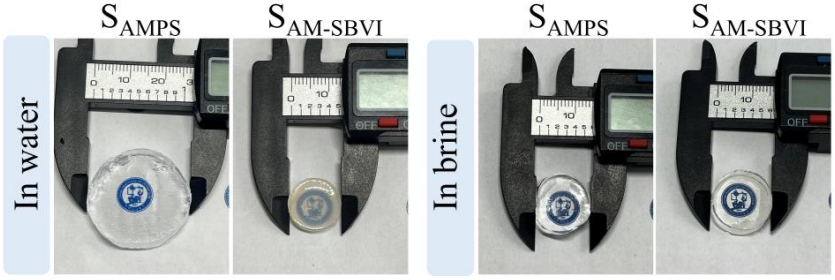

Figure R31. The morphological changes of S_{AMPS} and $S_{AM\text{-}SBVI}$ after swelling in water and brine (100 g/L NaCl).

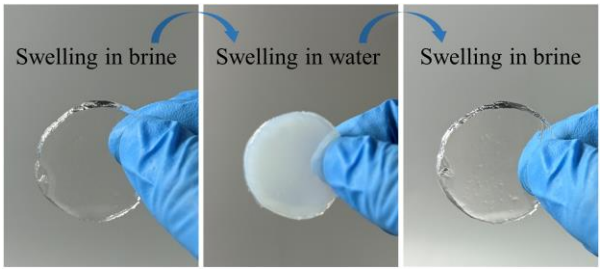

Figure R32. The morphological changes of $D_{AMPS/AM\text{-}SBVI}$ after swelling in water and brine (100 g/L NaCl).

We also measured the swelling ratio of different hydrogels in saline solution (100 g/L NaCl), as shown in Figure R33. The results show that S_{AMPS} exhibits the lowest swelling ratio due to the ionic shielding effect, which suppresses the osmotic pressure of the polyelectrolyte network. Benefiting from the anti-polyelectrolyte effect of SBVI, $S_{AM\text{-}SBVI}$ shows an increased swelling ratio. Notably, $D_{AMPS/AM\text{-}SBVI}$ displays the highest swelling ratio. This indicates that the enhanced swelling in brine is not reproduced by either single-network component alone, but emerges from their cooperative response within the interpenetrating double-network architecture. This synergistic effect may arise from: (1) the interpenetrating double-network structure preventing excessive contraction; (2) salt ions simultaneously shielding electrostatic interactions in the AMPS network and enhancing solvation of the SBVI network, generating synergistic swelling; and (3) the first network providing an elastic skeleton while the second network drives water absorption, collectively achieving the maximum swelling ratio.

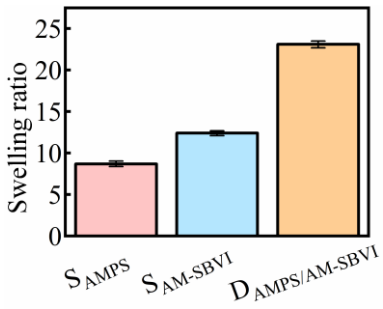

Figure R33. The swelling ratio of S_{AMPS}, $S_{AM\text{-}SBVI}$ and $D_{AMPS/AM\text{-}SBVI}$ after swelling brine (100 g/L NaCl).

We also investigate the rheological properties of different hydrogels in saline solution (100 g/L NaCl), as shown in Figure R34. The results demonstrate that $D_{AMPS/AM\text{-}SBVI}$ exhibits the highest G' and G'' compared to S_{AMPS} and $S_{AM\text{-}SBVI}$. We choose rheological comparison here because it provides a robust small-strain mechanical assessment for all saline-equilibrated gels, including the mechanically weaker single-network controls. This enhancement can be attributed to the synergistic reinforcement mechanism of the double-network structure: (1) the first AMPS network, pre-stretched during preparation, serves as a rigid skeleton providing high

elasticity; (2) the second AM-SBVI network, with its soft and stretchable chains and abundant topological entanglements, effectively dissipates energy through reversible breaking of sacrificial bonds; and (3) the interpenetrating architecture creates extensive interchain interactions, further increasing the overall network crosslinking density and mechanical robustness.

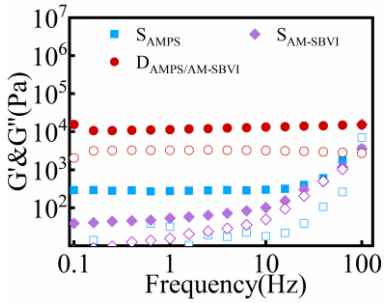

Figure R34. The rheological properties of S_{AMPS}, $S_{AM-SBVI}$ and $D_{AMPS/AM-SBVI}$ after swelling brine (100 g/L NaCl)

Taken together, these new comparisons clarify the key mechanism of our work more directly than the original Figure 1G. The single network controls reveal the individual brine response of the AMPS and AM-AMPS networks. The AMPS network alone is suppressed by ionic shielding, where the AM-SBVI network alone shows anti-polyelectrolyte-assisted swelling but limited mechanical reinforcement. Only when these two networks are integrated into the double-network architecture do we observe the simultaneous enhancement of swelling and mechanical properties. Therefore, the salt-enhanced behavior reported here does not originate from the well-known generic toughness advantage of double-network hydrogels alone, but from the synergistic coupling between the AMPS network and the zwitterionic AM-SBVI network under saline conditions, which enables salt-triggered structural reconfiguration and effective load-bearing reinforcement.

The relevant revised section has been highlighted in yellow in the manuscript and Supporting Information.

Reviewer #3 (Remarks to the Author):

In this manuscript, the authors developed an innovative ion-triggered reconfigurable hydrogel through a double network system composed of AMPS/AM-ABVI, fabricating DAMPS/AM-ABVI hydrogels. These hydrogels

demonstrated paradoxical salt-enhanced mechanical performance and swelling behavior. The researchers also provided an excellent mechanistic analysis of the salt-induced adaptive structural reorganization, revealing that inner-chain ion-pair loops dynamically unlock and reform as intra-network bridges (SBVI+-AMPS-) that serve as load-bearing elements under mechanical stress. Furthermore, the authors developed a temporary plugging agent based on DAMPS/AM-SBVI hydrogels and systematically investigated its coreflooding plugging efficiency and degradation performance, demonstrating its promising potential for applications in heterogeneous reservoirs, particularly under high-salinity and high-temperature conditions.

I think the work is very interesting and potentially worthy of publication in Nature Communications. However, the author still needs to revise the draft and answer some question prior to acceptance:

1. The text part needs to be double-checked. The phrase "A deep analysis concerts swelling/rheology into three descriptors, v_e, χ (Flory-Rehner inversion), and floop (loop fraction from bridge capacity)" needs clarification.

Thank you for your careful review. There is a spelling error of “concert”. The correct expression for this sentence is “A deep analysis converts swelling/rheology into three descriptors, v_e, χ (Flory-Rehner inversion), and f_{loop} (loop fraction from bridge capacity)”. We have reviewed the text part and conducted a double-check of the draft.

The relevant revised section has been highlighted in yellow in the manuscript and Supporting Information.

2. What were the theoretical or experimental bases for optimizing various parameters during the preparation of this DAMPS/AM-SBVI double-network hydrogel?

Thank you very much for your question. Our optimization strategy for the preparation conditions of $D_{AMPS/AM-SBVI}$ hydrogels adheres to the fundamental principles established by JianPing Gong for double-network (DN) hydrogels. Specifically, we follow the structural paradigm wherein the first network consists of abundantly cross-linked polyelectrolytes (rigid skeleton), while the second network

comprises poorly cross-linked neutral polymers (ductile substance)[45]. As demonstrated in prior studies[46], two critical structural parameters govern the mechanical strength of DN hydrogels. One is the molar ratio of the first to the second network, and the other is their crosslinking density. Accordingly, we systematically optimized the molar ratio of the two networks (Figure R35). Besides, incorporating dense entanglements to improve the mechanical strength[47], we optimize the cross-linker concentration for the second network, as shown in Figure R36. The weak physical interactions between networks of conventional DN hydrogels often compromise stress transfer upon brine swelling. To address this unique design, our system incorporates neutral and zwitterionic polymers in the second network, enabling intermolecular bonding with AMPS in the first network[48]. The optimization of the monomer content of the second network is shown in Figure R37.

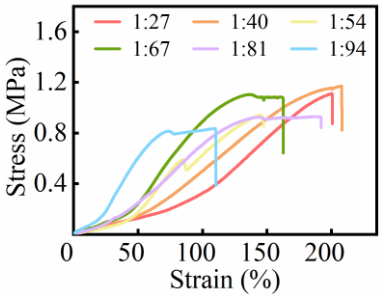

Figure R35. The optimization of the optimal molar ratio of the first network and the second network.

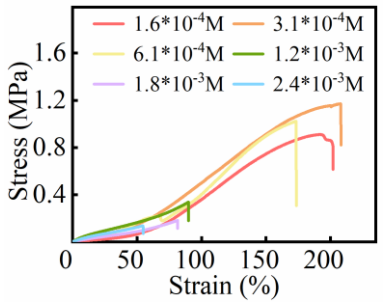

Figure R36. The optimization of the cross-linker concentration for the second network.

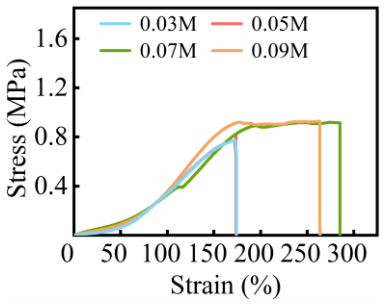

Figure R37. The optimization of the monomer content of the second network.

3. While SBVI is described as a laboratory-synthesized zwitterionic monomer, details regarding its synthesis procedure are notably absent in the manuscript.

Thank you for your careful review. The zwitterionic monomers (sulfobetaine vinylimidazole, SBVI) are synthesized by quaternization reaction following the modified procedures reported in the literature[49]. Vinylimidazole (0.2M) and 1,3-propane sultone (0.25M) are dissolved in acetonitrile. The mixture is thoroughly stirred, followed by purging with nitrogen gas to remove oxygen from the solution. Then, the flask is sealed and allowed to react at 40 °C for 24 h. After the reaction, the resulting precipitate is collected, washed with alcohol, and dried at 45 °C in the oven. The detailed synthesis procedure of SBVI is provided in the Preparation of zwitterionic monomers in the Supporting Information file. We have also annotated the relevant synthesis of SBVI in the manuscript and Supporting Information.

4. Why was the Flory-Rehner equation selected over alternative models (e.g., the Beltman-modified model) for χ parameter calculation? Does electrostatic shielding under high-salinity conditions potentially interfere with this model's applicability?

We appreciate your insightful question regarding the selection of the Flory-Rehner model. The Flory-Rehner equation is selected for its proven reliability in describing neutral or electrostatically screened polyelectrolyte networks, whereas the Beltman model is typically suitable for polyelectrolytes with unscreened electrostatic repulsion[25, 50]. In 100 g/L NaCl, Debye screening length is calculated as $\kappa^{-1}=\sqrt{\frac{\varepsilon_r\varepsilon_0 k_B T}{2N_A e^2 I}}$, which is about 0.96 nm[51]. From SAXS results, the radius of gyration *Rg* = 21.57 nm indicates a mesh size of approximately 55.7 nm in water, while brine

conditions expand this network. Critically, κ^{-1} is far smaller than the mesh size, confirming complete electrostatic screening and reducing the system to a pseudo-neutral network. Thus, the Flory-Rehner equation's applicability is validated. Based on this analysis, high salinity enables electrostatic shielding, fulfilling the prerequisite for Flory-Rehner's application. Furthermore, Beltman's model assumes unscreened electrostatic repulsion, contradicting our experimental data: (i) Structural transition from collapsed to expanded states; (ii) Dominant local ion-pairing.

5. What is the justification for setting ζ=1 in the equation ve=G'/ζRT?

Thanks for your question. According to the rubber elasticity theory[50], the effective bridge density (ν_e) could be calculated by $\nu_e=\frac{G'}{\zeta RT}$. In our double network hydrogel, the poorly cross-linked second network is the prominent part. This low-crosslinking-density architecture justifies our adoption of the phantom network model as the appropriate theoretical framework[52]. The parameter ζ represents the elastic front factor in the phantom network model and is determined by the crosslink functionality (f) through the relation ζ=1-2/f[53]. Our experimental system involves hydrogels that have undergone complete swelling in brine solution. Importantly, upon salt exposure, the hydrogel network experiences ion-triggered topological reorganization: the intrachain zwitterionic loops open and re-form as inter-network $SBVI^{+}$-$AMPS^{-}$ bridges, which yields a higher effective bridge density at lower polymer fraction. Due to the rapid bond recombination, crosslinking points cannot fluctuate freely, effectively increasing their instantaneous rigidity and maintaining topological constraints. Besides, the energy from bond rupture is rapidly dissipated through recombination rather than through chain segment motion (non-affine fluctuations)[52]. These combined effects justify our assignment of ζ = 1 for this system, despite employing the phantom network framework[54].

6. The equation needs to be double-checked, F_ion=RT∑_i▒〖c_i^b (e^(-z_i u) (-z_i u-1)〗 +1).

Thanks for your careful review. The correct equation is $F_{ion}=RT\sum_i c_i^b(e^{-z_i u}(-z_i u-1)+1)$. We have conducted a double-check of all equations.

7. 'SBVI++AMPS-' contains incorrect superscript/subscript formatting.

Thank you for your careful review. We have corrected this error and conducted rigorous verification of the text part.

8. Regarding free energy decomposition, what is the rationale for neglecting the Fdiss term? Detailed data supporting Figure 3L should be supplemented.

Given that the mean F_{tot} value exceeds 10^6 while F_{ion} averages only in the order of 10^2, the contribution of F_{ion} becomes negligible and can therefore be disregarded in our analysis. Detailed data of Figure 3L are shown in Table R1. The relevant revised section has been highlighted in yellow in the Supporting Information.

Table R1. The energy calculation results

Samples Parameters	F_{mix} (J/m^3)	F_{el} (J/m^3)	F_{assoc} (J/m^3)	F_{ion} (J/m^3)	F_{total} (J/m^3)
water	-2.94×10^6	4.46×10^4	-6.17×10^3	0	-2.9×10^6
20g/LNaCl	-2.74×10^6	5.32×10^4	-6.66×10^3	1.045×10^3	-2.692×10^6
100g/LNaCl	-2.65×10^6	8.61×10^4	-1.07×10^4	2.02×10^2	-2.574×10^6
200g/LNaCl	-2.41×10^6	1.22×10^5	-1.40×10^4	0.854×10^2	-2.302×10^6
Formation brine	-2.73×10^6	5.93×10^4	-3.38×10^3	1.09×10^2	-2.674×10^6

9. Numerous studies have also reported various functional zwitterionic hydrogels. To better highlight this work's novelty, a comparative analysis emphasizing the material's distinctive advantages over existing zwitterionic hydrogels should be included.

Thank you for your suggestion. We have systematically reviewed and compiled published studies on functional zwitterionic hydrogels presented in Table R2. The relevant revised section has been highlighted in yellow in the Supporting Information.

Table R2 Comparison of reported functional zwitterionic hydrogels

Topic	Novelty	Functional properties	Ref.
Ion-triggered reconfigurable hydrogels	Double network strategy: the first network is AMPS and the second network is AM-SBVI; network topological adaptation	Salt-enhanced mechanical and swelling properties	This paper
Salt-responsive hydrogels	Semi-interpenetrating double network: polycationic (polyMETAC/HEAA) layer with polyelectrolyte effect and polyzwitterionic (polyVBIPS) layer with antipolyelectrolyte effect	Enabling reversible bending actuation through differential dimensional change	55
Salt-responsive hydrogel	Double network strategy: loosely cross-linked zwitterionic pSBVI networks into the highly	Effective antimicrobial properties and surface regeneration.	56

	cross-linked cationic pTMAEMA		
Water-electricity co-generation gel	Molecularly engineered: incorporated phenyl-methylene-imidazole motif greatly enhances the salt binding ability and strengthens anti-polyelectrolyte effect	Boosted hydration, high salt tolerance, ultra-low evaporation enthalpy, durable anti-microbial ability, optimized water transport channel	2
Tough, non-swelling zwitterionic Hydrogel	Double network strategy: PVA, PSBMA; hofmeister-effect-assisted crystallization	Ultra-high toughness , non-swelling, long-term stability (>1 month) in harsh aquatic conditions	57
Electrochemical hydrogel	Molecularly engineered zwitterionic microgels as functional cross-linking domains within a highly entangled PAM network	Toughness 1450.8 kJ m^{-3}, low hysteresis, fatigue-resistant, conductivity 52.9 mS cm^{-1}, stable capacitance retention	58
Tough nonfouling zwitterionic hydrogels in saline	Pure zwitterionic triple-network with electrostatic interactions and entanglements as energy dissipation mechanisms	Compressive fracture stress of 18.2MPa in saline conditions, toughness of1.62 MJ m^{-3}, Young's modulusof 0.66 ± 0.03 MPa	59
Euryhaline hydrogels	Integration of two polymer segments with complementary salinity tolerances，internal dynamic complementary crosslinks	Stable water retention, constant swelling properties, and low-adhesion to oil in aqueous environments over a wide range of salinity.	60
Microphase-separated elastic ionic hydrogel	Double network strategy: zwitterions in the first network with highly entangled polymer chains; ultrasoft polyelectrolyte as the second network	Pressure sensitivity ~0.4 kPa^{-1}; temperature coefficient~1.5%·$°C^{-1}$, maintains stable signals under large strains and temperature fluctuations	48
Sulfonic-based zwitterionic hydrogel electrolyte	Directly exploit the Anti-Polyelectrolyte Effect of zwitterions to regulate the electrochemical stability window	Wide electrochemical stability window, high ionic conductivity , high working voltage, capacity, and energy density	1
Hygroscopic salt-hydrogel	Salting-in effect possessed by a zwitterionic hydrogel provide a new way to design more advanced composite sorbents	Facilitate water vapor sorption; enhanced swelling behavior in salt solutions	61

acrylamide (AM), poly([2-(methacryloyloxy)ethyl]trimethylammonium chloride) (polyMETAC), poly(3-(1-(4-vinylbenzyl)-1H-benzo[d]imidazol-3-ium-3-yl)propane-1-sulfonate) (polyVBIPS), poly(sulfobetaine vinylimidazole) (pSBVI), poly((trimethylamino)ethyl methacrylate chloride) (pTMAEMA), polyvinyl alcohol (PVA), poly(sulfobetaine methacrylate) (PSBMA), diallyldimethyl-ammonium chloride (DADMAC), polyacrylamide (PAM) poly(N-isopropylacrylamide) (PNIPAM).

10. Other minor: such as in Figure 2C, the pictures demonstrating the tensile stress-strain tests of swollen hydrogels are presented without a scale bar. Some figure caption needs to be double checked. In the supporting information, the

character of SBVI needs to be provide, such as NMR.

Thank you so much for your kindness and suggestions. We have reviewed all figures and added the necessary scale bar. We have reviewed the draft and conducted a double-check of all the figure captions. In this study, we select SBVI (a copolymer of propanesultone and vinyl imidazole, i.e., sulfobetaine vinyl imidazole) as the zwitterionic monomer, which is a sulfobetaine monomer containing an imidazolium cation structure. This design combines the advantages of sulfobetaine's inherent anti-polyelectrolyte effect with the enhanced physical interactions provided by the imidazolium cation. The NMR character of SBVI is shown in Figure R38 and we have added the NMR Figure in the Supporting Information.

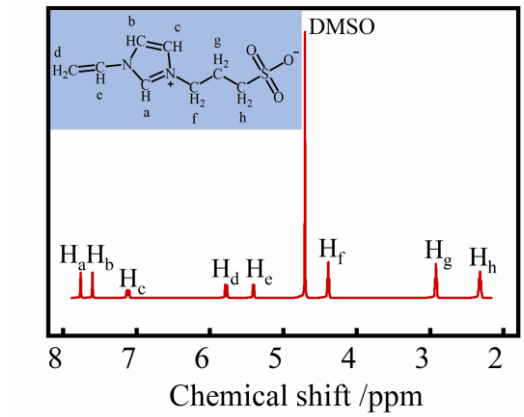

Figure R38. NMR characterization of SBVI

References

1. Zeng J, Chen H, Dong L, Guo X. Anti-Polyelectrolyte Effect of Zwitterionic Hydrogel Electrolytes Enabling High-Voltage Zinc-Ion Hybrid Capacitors. *Advanced Functional Materials* **34**, 2314651 (2024).

2. Zheng SY, *et al.* A Molecularly Engineered Zwitterionic Hydrogel with Strengthened Anti-Polyelectrolyte Effect: from High-Rate Solar Desalination to Efficient Electricity Generation. *Advanced Functional Materials* **33**, 2303272 (2023).

3. Cui K, *et al.* Phase Separation Behavior in Tough and Self-Healing Polyampholyte Hydrogels. *Macromolecules* **53**, 5116–5126 (2020).

4. Ohmura S, Oikawa K, Nishimura T, Kiyama R, Gong JP, Nakajima T. Osmosis-Induced Mechanical Disintegration of Polymer Network Gels. *Small* **21**, 2503209 (2025).

5. Jin X, Wei C, Wu C, Zhang W. Gastric fluid-induced double network hydrogel with high swelling ratio and long-term mechanical stability. *Composites Part B: Engineering* **236**, 109816 (2022).

6. Wu F, Pang Y, Liu J. Swelling-strengthening hydrogels by embedding with deformable nanobarriers. *Nature Communications* **11**, 4502 (2020).

7. Zhang K*, et al.* Dual role of divalent cations for enhanced low-temperature ionic conductivity and stability in zwitterionic hydrogel electrolytes. *Chemical Engineering Journal* **504**, 158855 (2025).

8. Cai J, Zhang L, Zhou J, Li H, Chen H, Jin H. Novel Fibers Prepared from Cellulose in NaOH/Urea Aqueous Solution. *Macromolecular Rapid Communications* **25**, 1558–1562 (2004).

9. Zhao YH*, et al.* Universal law of hierarchical dynamics in gels arising from confluence of local physically dynamic bonds. *Nature Communications* **16**, 3247 (2025).

10. Najafi Fath Dehghan H, Abdolmaleki A, Pourahmadi M, Khalili P, Arvaneh AR, Sadat-Shojai M. Highly conductive, anti-freezing, and adhesive hydrogels containing pores constructed by cation–dipole interactions. *Journal of Molecular Liquids* **382**, 121860 (2023).

11. Li F*, et al.* Self-Repairing and Damage-Tolerant Hydrogels for Efficient Solar-Powered Water Purification and Desalination. *Advanced Functional Materials* **31**, 2104464 (2021).

12. Chen M*, et al.* Sustainable and Rapid Water Purification at the Confined Hydrogel Interface. *Advanced Materials* **36**, 2311416 (2024).

13. Salunkhe B, Schuman T, Al Brahim A, Bai B. Ultra-high temperature resistant preformed particle gels for enhanced oil recovery. *Chemical Engineering Journal* **426**, 130712 (2021).

14. Najarbashi N, Baghban Salehi M, Saghandali F, Mokhtarani B, Mirzaei M, Sharifi A. Evaluation of the synergistic effect of nanocomposite hydrogel based on imidazolium nitrate ionic liquids for enhanced oil recovery. *Fuel* **377**, 132811 (2024).

15. Wang X-Q*, et al.* Structuring and Shaping of Mechanically Robust and Functional Hydrogels toward Wearable and Implantable Applications. *Advanced Materials* **36**, 2309952 (2024).

16. Naeem A*, et al.* Shape memory hydrogels in tissue engineering: Recent advances and challenges. *Bioactive Materials* **54**, 215–247 (2025).

17. Martinez-Moro M, Jenczyk J, Giussi JM, Jurga S, Moya SE. Kinetics of the thermal response of poly(N-isopropylacrylamide co methacrylic acid) hydrogel microparticles under different environmental stimuli: A time-lapse NMR study. *Journal of Colloid and Interface Science* **580**, 439–448 (2020).

18. Jin J*, et al.* An Extremely Salt-Resistant Hydrogel-Based Solar Evaporator for Stable Saturated Brine Desalination. *Small* **21**, 2411624 (2025).

19. Feng W, Wang Z. Tailoring the Swelling-Shrinkable Behavior of Hydrogels for Biomedical Applications. *Advanced Science* **10**, 2303326 (2023).

20. Stirnemann G, Wernersson E, Jungwirth P, Laage D. Mechanisms of Acceleration and Retardation of Water Dynamics by Ions. *Journal of the American Chemical Society* **135**, 11824–11831 (2013).

21. Liu K, Epsztein R, Lin S, Liu L, Qu J, Sun M. Electrostatic-driven dehydration of ions in nanoporous membranes. *Science Advances* **11**, eadv0174 (2025).

22. Alsaid Y*, et al.* Tunable Sponge-Like Hierarchically Porous Hydrogels with Simultaneously Enhanced Diffusivity and Mechanical Properties. *Advanced Materials* **33**, 2008235 (2021).

23. Li X*, et al.* Effect of Salt on Dynamic Mechanical Behaviors of Polyampholyte Hydrogels. *Macromolecules* **56**, 535–544 (2023).

24. Rubinstein M, Panyukov S. Elasticity of Polymer Networks. *Macromolecules* **35**, 6670–6686 (2002).

25. Flory PJ, Rehner J, Jr. Statistical Mechanics of Cross-Linked Polymer Networks I. Rubberlike Elasticity. *The Journal of Chemical Physics* **11**, 512–520 (1943).

26. Sun X, Mao Y, Yu Z, Yang P, Jiang F. A Biomimetic “Salting Out—Alignment—Locking” Tactic to Design Strong and Tough Hydrogel. *Advanced Materials* **36**, 2400084 (2024).

27. Hua M*, et al.* Strong tough hydrogels via the synergy of freeze-casting and salting out. *Nature* **590**, 594–599 (2021).

28. Graeber G*, et al.* Extreme Water Uptake of Hygroscopic Hydrogels through Maximized Swelling-Induced Salt Loading. *Advanced Materials* **36**, 2211783 (2024).

29. He S*, et al.* Nature-inspired salt resistant bimodal porous solar evaporator for efficient and stable water desalination. *Energy & Environmental Science* **12**, 1558–1567 (2019).

30. Zeng J, Wang Q, Shi Y, Liu P, Chen R. Osmotic Pumping and Salt Rejection by Polyelectrolyte Hydrogel for Continuous Solar Desalination. *Advanced Energy Materials* **9**, 1900552 (2019).

31. Jiang L-B*, et al.* Salt-Assisted Toughening of Protein Hydrogel with Controlled Degradation for Bone Regeneration. *Advanced Functional Materials* **29**, 1901314 (2019).

32. Si M*, et al.* Effect of Molecular Structures on Entanglements and Mechanics of Zwitterionic Hydrogels. *Macromolecules* **58**, 5516–5525 (2025).

33. Wang Z*, et al.* Recent advances in zwitterionic hydrogels: structure, applications and challenges. *Journal of Materials Chemistry A* **13**, 13693–13705 (2025).

34. Zheng SY*, et al.* Molecularly Engineered Zwitterionic Hydrogels with High Toughness and Self-Healing Capacity for Soft Electronics Applications. *Chemistry of Materials* **33**, 8418–8429 (2021).

35. Han J*, et al.* Bridge-rich and loop-less hydrogel networks through suppressed micellization of multiblock polyelectrolytes. *Nature Communications* **15**, 6553 (2024).

36. Xiao K, Kan C-M, Fan F-R, Parkin SSP, Cui X. Electrostatic screening of free charge-neutral dipoles/excitons in two-dimensional media. *Physical Review B* **112**, 165429 (2025).

37. Liu J*, et al.* Reconfiguring hydrogel assemblies using a photocontrolled metallopolymer adhesive for multiple customized functions. *Nature Chemistry* **16**, 1024–1033 (2024).

38. Liu P*, et al.* Hydrogel-Reactive-Microenvironment Powering Reconfiguration of Polymer Architectures. *Advanced Science* **11**, 2307830 (2024).

39. Yuan Z*, et al.* Ultra-robust, repairable and smart physical hydrogels enabled by nano-domain reconfiguration of network topology. *Chemical Engineering Journal* **450**, 138085 (2022).

40. He H*, et al.* Zwitterionic hydrogels from material design to wound dressing applications. *Supramolecular Materials* **4**, 100108 (2025).

41. Xiao S*, et al.* Salt-responsive zwitterionic polymer brushes with anti-polyelectrolyte property. *Current Opinion in Chemical Engineering* **19**, 86–93 (2018).

42. Xiao S*, et al.* Structural Dependence of Salt-Responsive Polyzwitterionic Brushes with an Anti-Polyelectrolyte Effect. *Langmuir* **34**, 97–105 (2018).

43. Liang C*, et al.* Stiff and self-healing hydrogels by polymer entanglements in co-planar nanoconfinement. *Nature Materials* **24**, 599–606 (2025).

44. Fu L*, et al.* Cartilage-like protein hydrogels engineered via entanglement. *Nature* **618**, 740–747 (2023).

45. Gong JP, Katsuyama Y, Kurokawa T, Osada Y. Double-Network Hydrogels with Extremely High Mechanical Strength. *Advanced Materials* **15**, 1155–1158 (2003).

46. Gong JP. Why are double network hydrogels so tough? *Soft Matter* **6**, 2583–2590 (2010).

47. Kim J, Zhang G, Shi M, Suo Z. Fracture, fatigue, and friction of polymers in which entanglements greatly outnumber cross-links. *Science* **374**, 212–216 (2021).

48. Liu X, Ji X, Zhu R, Gu J, Liang J. A Microphase-Separated Design toward an All-Round Ionic Hydrogel with Discriminable and Anti-Disturbance Multisensory Functions. *Advanced Materials* **36**, 2309508 (2024).

49. Carr L, Cheng G, Xue H, Jiang S. Engineering the Polymer Backbone To Strengthen Nonfouling Sulfobetaine Hydrogels. *Langmuir* **26**, 14793–14798 (2010).

50. Rubinstein M, Colby RH. *Polymer Physics*. Oxford University Press (2003).

51. Blees M. Foundations of Colloid Science. *Colloids and Surfaces A: Physicochemical and Engineering Aspects* **210**, 125 (2002).

52. Rubinstein M, Panyukov S. Nonaffine Deformation and Elasticity of Polymer Networks. *Macromolecules* **30**, 8036–8044 (1997).

53. Flory PJ. Theory of elasticity of polymer networks. The effect of local constraints on junctions. *The Journal of Chemical Physics* **66**, 5720–5729 (1977).

54. Van Gunsteren WF, Karplus M. Effect of constraints on the dynamics of macromolecules. *Macromolecules* **15**, 1528–1544 (1982).

55. Xiao S*, et al.* Salt-Responsive Bilayer Hydrogels with Pseudo-Double-Network Structure Actuated by Polyelectrolyte and Antipolyelectrolyte Effects. *ACS Applied Materials & Interfaces* **9**, 20843–20851 (2017).

56. Huang K-T, Ishihara K, Huang C-J. Polyelectrolyte and Antipolyelectrolyte Effects for Dual Salt-Responsive Interpenetrating Network Hydrogels. *Biomacromolecules* **20**, 3524–3534 (2019).

57. Ren J*, et al.* Super-Tough, Non-Swelling Zwitterionic Hydrogel Sensor Based on the Hofmeister Effect for Potential Motion Monitoring of Marine Animals. *Advanced Materials* **36**, 2412162 (2024).

58. Ni H, Wang S, Wang C, Wang G, Zheng SY, Yang J. Zwitterionic Microgel-Reinforced Hydrogels with Low Hysteresis and High Toughness for Electrochemical Applications. *ACS Applied Materials & Interfaces* **18**, 4283–4292 (2026).

59. Li X*, et al.* High-Strength and Nonfouling Zwitterionic Triple-Network Hydrogel in Saline Environments. *Advanced Materials* **33**, 2102479 (2021).

60. Gao H*, et al.* Euryhaline Hydrogel with Constant Swelling and Salinity-Enhanced Mechanical Strength in a Wide Salinity Range. *Advanced Functional Materials* **31**, 2007664 (2021).

61. Aleid S*, et al.* Salting-in Effect of Zwitterionic Polymer Hydrogel Facilitates Atmospheric Water Harvesting. *ACS Materials Letters* **4**, 511–520 (2022).